# RobustSurg: Tackling domain generalisation for out-of-distribution surgical scene segmentation

Mansoor Alia, Maksim Richards, Gilberto Ochoa-Ruiz\* and Sharib Ali\*c

#### ABSTRACT

While recent advances in deep learning (DL) for surgical scene segmentation have demonstrated promising results on single-centre and single-imaging modality data, these methods usually do not generalise to unseen distribution (i.e., from other centres) and unseen modalities. Even though human experts can distinguish visual appearances, DL methods often fail to do so if data samples do not follow the independent and identically distributed (IID) data property, where IID refers to the data samples drawn from the same distribution. Current literature for tackling generalisation on out-ofdistribution (OOD) data and domain gaps due to modality changes has been widely researched but mostly for natural scene data. However, these methods cannot be directly applied to the surgical scenes due to limited visual cues and often extremely diverse scenarios compared to the natural scene data. Inspired by these works in natural scene to push generalisability on OOD data, we hypothesise that exploiting the style and content information in the surgical scenes could minimise the appearances making it less variable to sudden changes such as blood or imaging artefacts. This can be achieved by performing instance normalisation and feature covariance mapping techniques for robust and generalisable feature representations. Further, to eliminate the risk of removing salient feature representation associated with the objects of interest, we introduce a restitution module within the feature learning ResNet backbone that can enable the retention of useful task-relevant features. To tackle lack of multiclass and multicentre data for surgical scene segmentation, we also provide a newly curated dataset that can be vital for addressing generalisability in this domain. Our proposed RobustSurg obtained nearly 23% improvement on the baseline DeepLabv3+ and from 10-32% improvement on the SOTA in terms of mean intersection over union (IoU) score on an unseen centre HeiCholSeg dataset when trained on CholecSeg8K. Similarly, RobustSurg also obtained nearly 22% improvement over the baseline and nearly 11% improvement on a recent state-of-the-art (SOTA) method for the target (different modality) set of EndoUDA polyp dataset.

## 1. Introduction

Minimally invasive surgery (MIS) has brought about a paradigm shift in modern surgical practice by reducing hospitalisation time, operative trauma, visible scars, and the risk of comorbidity (Buia et al., 2015). However, the quality of a surgical procedure in the traditional operating room still largely depends on the surgical proficiency and experience of the surgeon. Moreover, the conditions and safety requirements during surgery can be quite demanding for the persons involved. Thus, AI tools have been developed to assist in interventions for tasks such as surgical tool navigation (Xu et al., 2023), skill assessment (Igaki et al., 2023), workflow analysis (Zhang et al., 2023), and action recognition (Sharma et al., 2023), among others.

Image-guided procedures such as laparoscopic, endoscopic and radiological interventions heavily rely on images for surgical guidance and decision support. With the global expansion of minimally-invasive surgical practice and the number of surgeries performed, the volume of acquired video data is increasing rapidly. The recent success of deep learning approaches are the perfect avenues to use this data

\*Corresponding author(s): Gilberto Ochoa-Ruiz (gilberto.ochoa@tec.mx) Sharib Ali ( s.s.ali@leeds.ac.uk) ORCID(s): to further help clinicians in decision making, thus improving patient safety and healthcare.

In MIS, the subconscious assumptions typical of human visual perception can lead to erroneous interpretations of endoscopic and radiological images, contributing to serious adverse events such as bile duct injuries that were rarer during traditional, open surgery procedures (Mascagni et al., 2022). Therefore, understanding the surgical scene objectively can result in improved surgical outcomes.

Surgical scene semantic segmentation enables precise identification of anatomical structures and instruments, providing contextual information for comprehensive surgical scene understanding. Semantic segmentation partitions raw image data into structured and meaningful regions and thus enables further image analysis and quantification, which are critical for various applications, including anatomy research, disease diagnosis, treatment planning, and intra-operative decision support. Understanding the surgical scene via full scene segmentation is a prerequisite for many assistance functions in computer-assisted interventions (CAI), such as robotic assisted surgery and surgical workflow analysis. Surgical scene understanding can provide real-time surgical assistance in the operating room, thus improving the safety and efficacy of the procedure.

A vast majority of existing state-of-the-art (SOTA) computer vision models (Yoon et al., 2022; Grammatikopoulou

<sup>&</sup>lt;sup>a</sup>Escuela de Ingenieria y Ciencias, Tecnologico de Monterrey, Monterrey, 64849, N.L., Mexico

<sup>&</sup>lt;sup>b</sup>St John's College, University of Oxford, Oxford, OX1 3JP, UK

<sup>&</sup>lt;sup>c</sup>School of Computer Science, University of Leeds, Leeds, LS2 9JT, UK

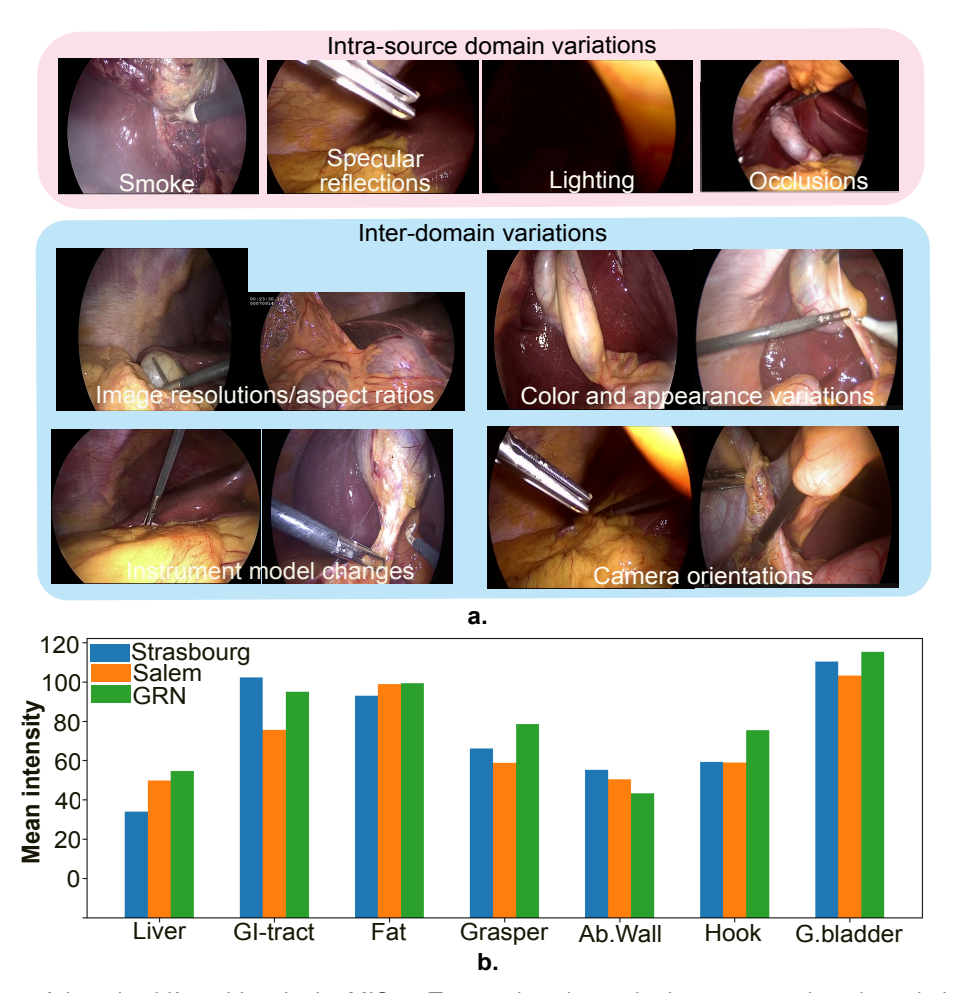


**Figure 1:** Overview of domain shift problem in the MIS. **a.** Top section shows the intra-source domain variations which we aim to exploit in learning a generalisable model, while bottom section shows shift problem between source and target domains. **b.** Comparison of intensity histograms between training source domain and different centre target domains.

et al., 2024) for surgical scene segmentation assume training and test data as independent and identically distributed (IID) i.e., data from same distribution. However, in real world settings, deploying models trained on data from one healthcare centre will suffer from performance degradation on data from other centres due to the domain shift caused by various factors such as patient demographics, instrument types, and vendor choice of the system to acquire the data. Fig. 1(a) shows some of the intra-source and inter-domain variations separately. Typical endoscopic artifacts include the presence of smoke, specular reflections, illumination changes, and occlusions. Inter-domain variations comprise changes of aspect ratio between source and target data, photometric changes, changes in instrument types and vendors, and camera recording orientation. Fig. 1(b) shows how color intensity distributions change across various healthcare centre datasets which inevitably can impact cross-centre model performance. Furthermore, complications during surgical procedures, lighting conditions, surgeon expertise levels can also append to the domain shift resulting in even lower model performance. Work on domain-generalised surgical methods have been quite limited due to the unavailability

of diverse multicentre annotated datasets. In this work, we aim to address these two important challenges, i.e., model generalisability and lack of multicentre annotated data.

Efforts towards developing approaches for generalisable methods for surgical domain has recently gained attention with few studies (Murali et al., 2023; Wagner et al., 2023) published to tackle this problem. The advancements in this area of research have focused on two fronts: algorithmic and multicentre data collection level. On the algorithmic level, only the SOTA methods (Wang et al., 2023; Satyanaik et al., 2024) from the natural computer vision domain have been tested on a limited out-of-distribution (OOD) settings which fail to learn enough discriminative features from the training data limiting their capability to generalise well on the unseen distribution. On the multicentre data collection too, the progress has been limited, where in some cases, data has not been released publicly Satyanaik et al. (2024) to encourage further research and enable the research community to assess the generalisability of methods.

Therefore, the question we aim to answer is can we design ML models that can perform optimally on the IID samples but minimise performance degradation when OOD

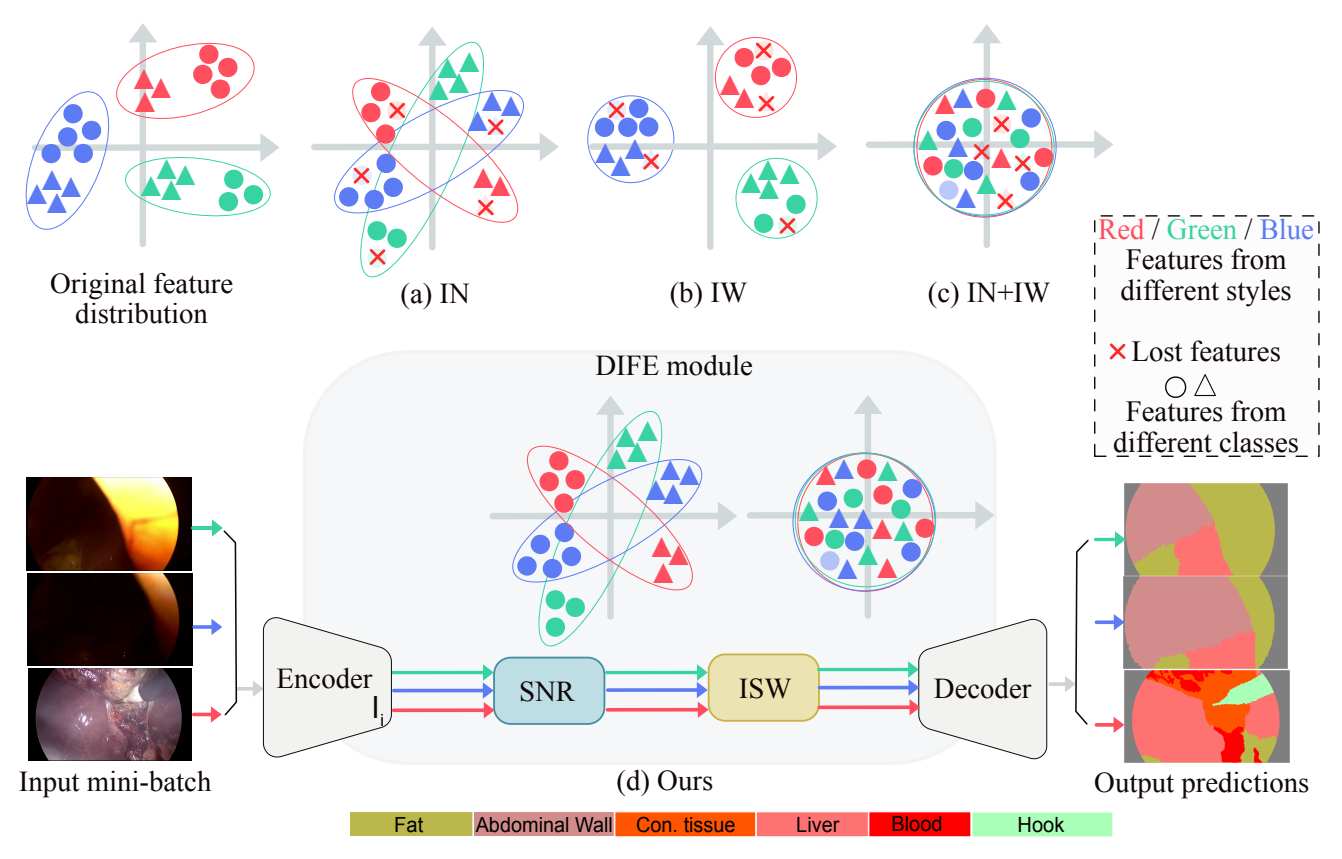


**Figure 2:** Comparative illustration of existing DG approaches and our proposed approach. Current Instance normalization (IN) and Instance whitening (IW) techniques (a-c) performs feature standardization and minimise global distribution variance but also loose some useful discriminative information (shown with faded symbols). Our proposed Domain-invariant feature encoder (DIFE) block aims to restore the lost features during IN stage. Note that this figure shows features from two classes for simplicity, but the idea applies to all classes.

samples are encountered, i.e., generalisable to arbitrary unseen samples or distribution? A generalisable model also alleviates the need of requiring access to multicentre data for training, which is otherwise unfeasible due to data protection and privacy restrictions.

To tackle the generalisability problem in semantic segmentation, several works have been carried out in the traditional computer vision (i.e., natural scenes). To this end, IBN-Net (Pan et al., 2018) combined batch and instance norm to learn domain-invariant features. Following this approach, several other methods have also used instance norm along with other feature learning blocks like feature whitening (Choi et al., 2021), category level learning Peng et al. (2022), style diversification (Lee et al., 2022), covariance alignment (Ahn et al., 2024). Although these methods have been successful in learning domain-invariant information, such techniques have not been widely explored in surgical computer vision settings. In this paper, we aim to bring the successes of existing DG approaches to the surgical domain to effectively learn domain discriminative features. Prior works (Pan et al., 2018; Choi et al., 2021) have shown the effectiveness of using instance norm (Ulyanov et al., 2016) in DG, however, IN alone is not adequate on two counts -1) It merely standardises the features while also inevitably

removing discriminant features (Ahn et al., 2024; Jin et al., 2021) as shown in Fig. 2(a)., and 2) it does not take into account the correlation between channels. The loss of discriminative information due to IN is further compounded in subsequent works using Instance whitening (Fig. 2(b).) and the combination of Instance norm and whitening (Fig. 2(c).). Furthermore, current DG approaches work in a multisource domain setting where multiple source domains are available for training. However, obtaining multiple labeled datasets is unfeasible for training especially in the surgical domain.

To address the above mentioned issues, we propose a RobustSurg, a single domain generalization approach to tackle domain generalization in the surgical domain by learning from one source domain. RobustSurg consists of a novel Domain-invariant feature encoder (DIFE) block that integrates style normalization and restitution (SNR) and instance selective whitening (ISW) block into the three convolution layers of ResNet-50 backbone to boost DG performance (Fig. 2(d).). SNR applies IN after the convolution layers to eliminate style variations and restores the discriminant features. Since feature covariance contains domain-specific information such as texture and color (Gatys et al., 2016, 2015), the ISW block exploits the feature covariances

from the original and augmented images through a whitening transformation (WT) (Cho et al., 2019) to selectively remove the style information and retain the structure and content.

Furthermore, a general lack of annotated multicentre test data to evaluate model generalization has been the singlemost important bottleneck in the surgical DG domain. We overcome this limitation by taking a part of HeiChole Benchmark (Wagner et al., 2023) dataset comprising of data from two healthcare centres and labeling it with the scene segmentation labels, rigorously reviewed by an in-house clinical expert. We developed an annotation protocol based on the expert recommendations for cholecystectomy surgeries discussed in Mascagni et al. (2021) and then a senior postgraduate student performed the pixel-wise labeling of the data followed by rigorous review conducted by an inhouse clinical expert. We evaluated the effectiveness of our approach on both in-domain test sets (i.e., IID) and on different modalities and different centre datasets (i.e., OOD). Specifically, we train the network on CholecSeg8k (Hong et al., 2020) dataset and test on our newly introduced multicentre test set. We will release both the implementation code and dataset upon acceptance of our work. To further validate model generalisability performance, we conducted model training and testing on two other dataset settings. One on multimodality EndoUDA dataset and another on cross-centre cataract surgery datasets. The EndoUDA (Celik et al., 2021) dataset is comprised of white-light imaging (WLI) and narrow-band imaging (NBI) for polyps and Barrett's esophagus. WLI and NBI differ markedly in color distribution, contrast, and texture due to their distinct optical principles, with NBI emphasizing vascular and mucosal patterns through narrow wavelength illumination. Testing a WLI-trained model on NBI serves as a strong evaluation setup of cross-modality generalisability, assessing robustness to significant domain shifts common in realworld surgical deployments. Second, we conducted crosshospital experiments on cataract surgery data and present results of a model trained on CaDIS dataset (recorded at the Brest university hospital) and tested on cataract-1K dataset (record at eye clinic of Klinikum Klagenfurt). We present evaluation results on different evaluation metrics such as mean Intersection over union (mIoU), precision, recall and pixel accuracy. We also provide per-class results to see how model behaves on instruments and anatomical regions. Further, we also perform different ablation experiments to see the effectiveness of various ISW and SNR blocks. Our major contributions are summarised below.

- We introduce a newly annotated cholecystectomy dataset with 8 classes from two surgical centres to rigorously test the domain generalization for surgical scene segmentation.
- We propose a novel domain-invariant feature encoder to address the loss of discriminant information from features in widely used instance normalization technique.

We validate our proposed approach for generalisability on three surgical datasets. Our experiments demonstrate that our approach is superior to other state-of-the-art approaches.

The rest of the paper is organised as follows. Detailed related work on Domain generalization in natural and surgical domain and discussion about lack of diverse datasets is discussed in Section 2. Details of our new multicentre dataset and method are explained in Section 3. Section 4 presents the implementation details, experimental setup and the description of evaluation metrics used. Results are comprehensively presented and discussed in Section 5. Finally, conclusion and future work is presented in Section 6.

#### 2. Related Work

Learning domain-agnostic models from limited source domain data is an important area of investigation in several fields, including computer vision at large and medical imaging in particular. In this section, we revisit some of the related works in the field domain generalization in natural and medical image scenarios.

**Domain Generalization.** Domain generalization aims to extract domain-invariant features from source domain(s) to learn a generalisable representation better-suited for unseen target domains. DG methods can be broadly categorised into three different groups: (i) Representation learning techniques that aim to extract domain-invariant knowledge from the source domain(s) that seamlessly generalise to any arbitrary target domain (Blanchard et al., 2011; Nguyen et al., 2021). (ii) Data augmentation methods learn to diversify the source domains to have more representative training data (Gong et al., 2019; Zhou et al., 2020, 2021) (iii) Learning-strategy approaches may achieve generalization through meta-learning (Wei et al., 2021), self-supervised learning (Carlucci et al., 2019), causality learning (Sun et al., 2021) or optimization procedures (Cha et al., 2021) aimed at finding a flat minima. In this work, we approach the DG problem using the representation learning approach where we aim to separate the style and content information learn the generalisable representation.

**Style-Content Disentanglement.** S-C disentanglement aims to partition the aggregated latent variables into two separate components, denoted as style and content. While the concepts of style and content have their origins in the style transfer literature (Mathieu et al., 2016; Szabó et al., 2017), recent studies have further advanced the concept by incorporating the approaches like causal inference (Peters et al., 2017), independent component analysis (Gresele et al., 2021), and feature covariance (Choi et al., 2021). CDDSA (Gu et al., 2023) proposed separate anatomy encoder and modality encoder to disentangle style-content features and used the decoder to reconstruct the final prediction. Style-semantic contrastive loss was proposed to disentangle the source and target stylised features (Guo et al., 2023). Style-content disentanglement was tackled by adding covariance alignment modules in the encoder and

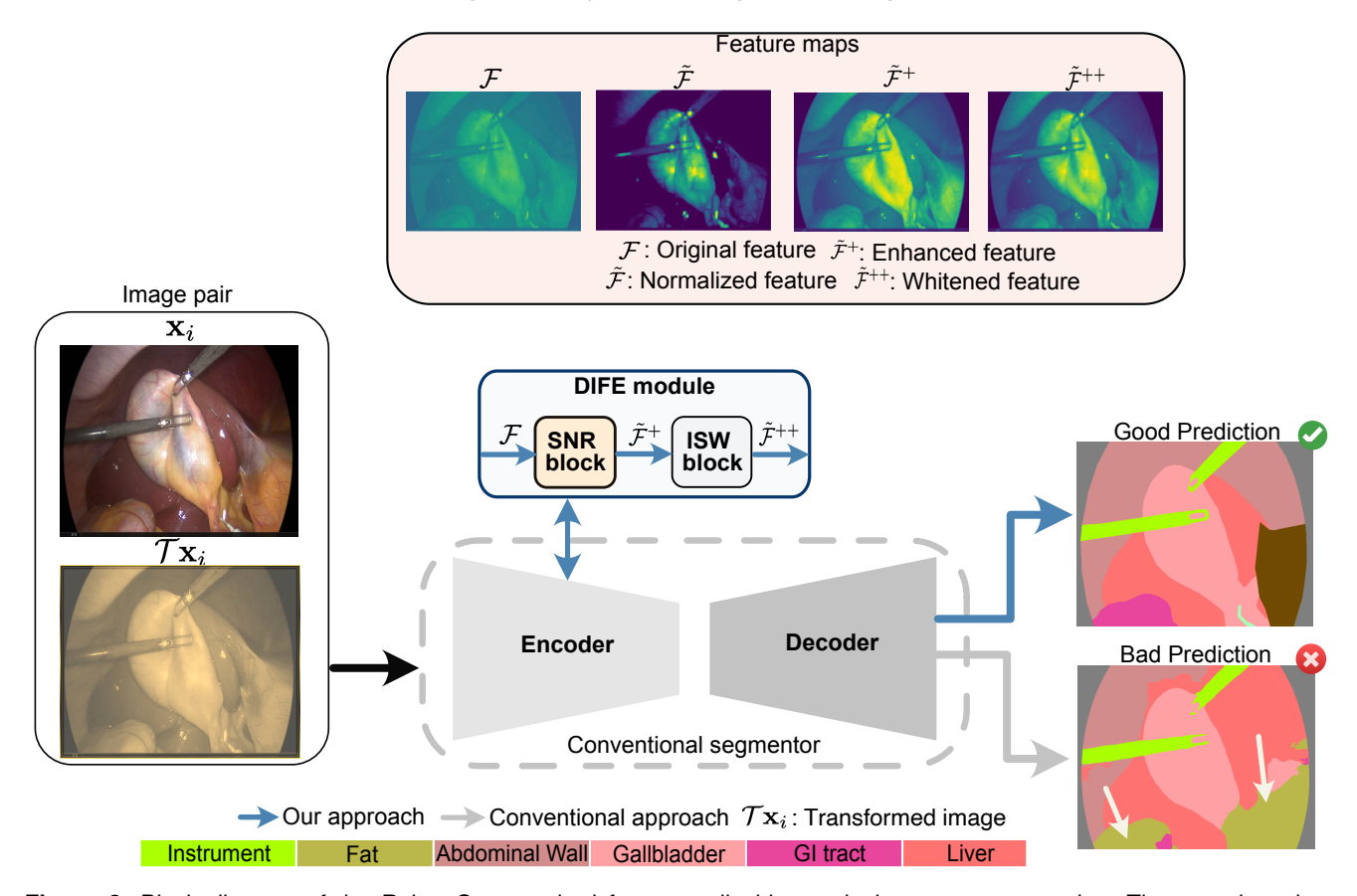


**Figure 3:** Block diagram of the RobustSurg method for generalisable surgical scene segmentation. The encoder takes two images, i.e., raw image and transformed image. Conventional segmentors such as DeepLabv3+ (Chen et al., 2018) underperform on unseen images as shown in the prediction. In our approach, we introduce domain-invariant feature encoder (DIFE) module containing two sub-blocks. SNR block (Jin et al., 2021) normalises and recovers the lost features while ISW block selectively suppresses the style information.

contrastive learning in the decoder for DGSS (Ahn et al., 2024). In a multisource DG settings (Lee et al., 2022) where multiple source domains are employed as training data, disentanglement of domain-invariant features have shown great potential in training robust deep learning models by leveraging shared knowledge across domains. On the contrary, disentanglement has been rarely studied in single DG (sDG) setting where just one source domain is available for training.

Previous literature in sDG (Gatys et al., 2016; Choi et al., 2021) reveal that feature correlation (i.e., a covariance matrix) stores the domain-specific styles of images. Specifically, the whitening transformation has shown success in removing feature correlation and domain-specific style information in image translation (Cho et al., 2019), style transfer (Li et al., 2017), domain adaptation (Roy et al., 2019) and generalization (Choi et al., 2021), thus improving model generalisability. It has also been shown that instance normalization (IN) in shallow layers of CNNs boost model's ability to learn discriminant features (Pan et al., 2018; Nam and Kim, 2018). However, explicit use of IN can result in loss of discriminant information, since it is task-agnostic. Building upon previous work on feature disentanglement

(Jin et al., 2021) and feature whitening (Choi et al., 2021), we aim to disentangle style-content information in a sDG setting for surgical scene segmentation using the combination of feature covariance and style restitution to improve DG performance.

**Domain generalization in surgical domain.** Domain generalization has largely been an under-explored topic in surgical domain. There are only a few studies conducted on learning domain-agnostic models for surgical instrument localization (Philipp et al., 2022, 2021), scene understanding (Seenivasan et al., 2022), object-centric learning (Satyanaik et al., 2024), and endoscopic image segmentation (Guo et al., 2024). Despite the initial efforts, DG in the surgical domain remains methodologically underexplored, with limited efforts targeting domain-agnostic learning for critical tasks such as full scene segmentation. In terms of datasets, the Heidelberg colorectal dataset which was successfully used in the Robust-MIS (Ross et al., 2020) challenge was the first comprehensive multicentre dataset to assess model generalisability for instrument detection and segmentation under challenging surgical images. Bar et al. (2020) investigated the generalisability of surgical workflow recognition task on a multicentre surgical dataset showing

that training models on diverse datasets can potentially enable translating AI research into the clinical practice. Although these datasets are based on clinical patient videos for their annotations, their applicability is limited, as they do not adequately capture the variability of clinical data across multiple centres and focus on only on specific features of the surgical images (e.g surgical instruments). To address these limitations, the Heichole multicentre dataset (Wagner et al., 2023) was initially introduced for surgical workflow analysis, and skill assessment and later used in EndoVis 2021 challenge for surgical scene segmentation. However, the scene segmentation annotations were not publicly released.

The lack of model generalization works in surgical domain can be partly attributed to the scarcity of labeled multicentre datasets for model evaluation. One line of work to address data scarcity problem in surgical domain has proposed diffusion models to generate diverse annotated datasets (Venkatesh et al., 2025). However, recent research (Akbar et al., 2025) has shown that instead of learning the structure of data, diffusion models are more prone to learn the training data itself and do not produce diverse data. We derive our motivation from this important observation and introduce an annotated multicentre dataset by taking publicly available HeiChole multicentre videos (Wagner et al., 2023) and annotating with semantic segmentation labels for testing model generalisability in terms of surgical scene segmentation.

Limitations. While Domain generalization has witnessed growing interest in the natural image domain, its applications to the surgical domain still remain underdeveloped in terms of methodological rigor and lack of data diversity. Existing efforts in surgical domain have largely focused on a few tasks such as instrument localization, or segmentation, but they lack robust frameworks for generalization across diverse surgical environments. In this work, we aim to adapt Style-content disentanglement, one of the effective approaches in natural DG to the surgical domain and aim to alleviate the loss of information due to instance normalization with feature restitution.

A great obstacle in developing generalisable methods for laparoscopic surgery is the lack of diverse multicentre datasets. To address this gap and to encourage further research, we release HeiCholeSeg, a pixel-wise annotated dataset from two different surgical centres for generalisability evaluation of deep learning models. To summarise, domain-agnostic approaches tailored to the domain shifts in surgical data, alongwith multicentre annotated datasets are needed to further advance the research in surgery.

# 3. Materials and Method

In this section, we first delve into the details of the novel HeiCholeSeg, multicentre annotated dataset, and the annotation and validation process. The next part of the section presents the RobustSurg method.

# 3.1. Novel multicentre annotated surgical dataset

We introduce HeiCholeSeg, a multicentre pixel-wise annotated dataset to address the limitation of lack of diverse, representative and annotated datasets in the surgical domain. The HeiCholeSeg dataset is taken from the public HeiChole Benchmark (Wagner et al., 2023) which consists 24 public videos of laparoscopic cholecystectomies performed at three German hospitals. The videos at Heidelberg University Hospital were recorded with a laparoscopic 2D camera (Karl Storz SE & Co KG, Tuttlingen Germany), and at Salem and GRN-hospital Sinsheim hospitals, they were recorded with the laparoscopic 2D camera ENDOCAM Logic HD (Richard Wolf GmbH, Knittlingen, Germany). Originally, the dataset was frame-wise annotated with surgical phases, actions, instrument presence and skills but did not include segmentation masks.

A subset of frames was selected for annotation, since annotating all 24 videos would have resulted in more than 10 million images and an impractical labeling effort. To this end, two full surgery videos (each having duration of nearly an hour and each from Salem and GRN hospitals) were selected for the HeiCholeSeg data based on the annotation capacity. Details regarding the dataset characteristics can be found in Table 1 and some example frames are provided in Fig. 4. To ensure consistency and surgical phase alignment between training and test datasets, an expert clinician manually selected the relevant temporal segments of each video. These segments correspond specifically to the cholecystectomy phase of the surgery. This step was crucial for creating a consistent benchmark across institutions and to match the training dataset phases. From the selected video segments, frames were extracted at a fixed sampling rate of 25 frames per second (fps) (with a custom python script). This rate was chosen to balance annotation burden and frame data variability. A fourth year postgraduate student having 4 years of experience in artificial intelligence in surgical image analysis guided by a medical expert with over 6 years of experience proceeded with the labeling task. Annotation was performed using Wacom tablets to facilitate precise and efficient pixel-level delineation of semantic classes on Labelbox (Labelbox, 2024), an opensource collaborative web-based tool.

The annotator was required to annotate all the semantic classes including anatomical structures and surgical instruments in the frames. The annotator conducted the initial round of annotations on selected frames from cholecystectomy videos from each centre. The medical expert reviewed the annotated data, providing detailed feedback and comments on instances of potential mislabeling, ambiguity, or anatomical/surgical inaccuracy. Based on the expert's feedback, the annotations were revised to correct the class delineations and anatomy class assignments. The revised annotations underwent a second round of review by the medical expert who provided feedback on any remaining inconsistencies. The flagged instances were returned to the annotator for a second re-annotation. Following this reannotation, the medical expert performed final validation

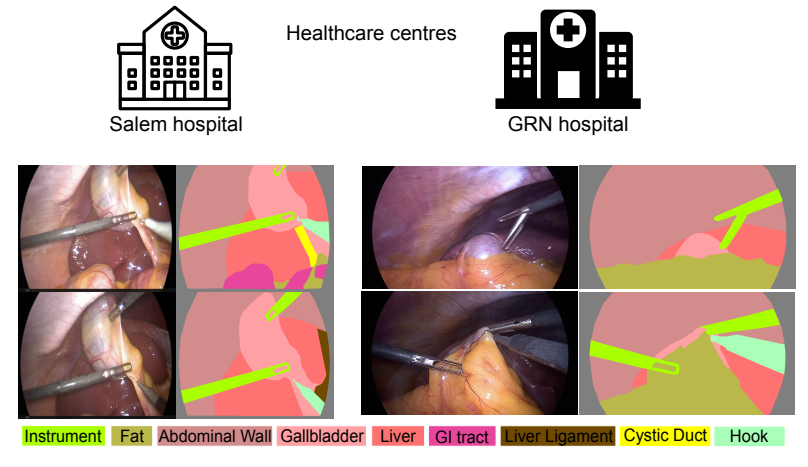


**Figure 4:** Example from the HeiCholeSeg multicentre dataset. Each image is shown alongwith its corresponding semantic segmentation mask. Images depict varying photometric properties, and aspect ratios across the surgical centres.

**Table 1**Overview of data acquisition settings across different medical centres. Note that CholecSeg8k data was recorded at Strasbourg centre.

|                 | Data Centre              | Laparoscope  | Resolution  | FPS | # of images |
|-----------------|--------------------------|--|-------------|-----|-------------|
| <br> eiCholeSeg | Salem hospital           | 2D camera ENDOCAM Logic HD (Richard Wolf GmbH, Knittlingen, Germany) with 30° optics | 720 × 576   | 50  | 150         |
| HeiCl           | GRN-hospital<br>Sinsheim | 2D camera ENDOCAM Logic HD (Richard Wolf GmbH, Knittlingen, Germany) with 30° optics | 1920 × 1080 | 50  | 150         |
|                 | Strasbourg centre        |  | 480 × 854   | 25  | 8080        |

of the annotations. Although some delineation errors are inevitable given the inherent complexity of segmentation tasks, our iterative, multistage annotation protocol substantially reduced these errors, resulting in high-quality and reliable annotations.

Detailed annotation instructions as well as class definitions were determined and communicated in the annotation protocol. Some of the general rules for the annotation task are as follows:

- The cystic duct and the cystic artery are two tubular structures which are connected to the gallbladder.
- Gallbladder is a pear-shaped organ located beneath the liver, appears as grey-blue sac attached to the liver surface.
- Liver is a large reddish-brown organ occupying the right upper abdomen, partially visible above the gallbladder.
- Segment the region visible through the fenestrated jaws of instruments such as grasper.

#### 3.2. Method

The main goal of this work is to train a semantic segmentation model on source domain (surgical endoscopic

data from one distribution or a healthcare centre) which generalises well on target domain (unseen distribution or different healthcare centre), performing better than the baseline conventional model i.e., DeepLabv3+ (Chen et al., 2018). Conventional segmentation models lack the ability to learn sufficiently discriminative features from the training data hence their performance severely degrades when tested on OOD data. Therefore, we tackle this problem by introducing a plug-and-play domain-invariant feature encoder (DIFE) block which which can be plugged to any backbone network such as ResNet50 of DeepLabv3+. Fig. 3 shows the overall proposed framework of RobustSurg and its comparison to conventional models for semantic segmentation. The DIFE module in our proposed method consists of two blocks adapted from the state of the art to the surgical domain, Style normalization and Restitution (SNR) (Jin et al., 2021), and instance selective whitening (ISW) (Choi et al., 2021). The DIFE module works by performing three operations on each feature map passed from an encoder layer. The first task being style normalization through instance norm, the second task is the restitution operation to restore the discriminant information lost during instance norm, and then finally the whitening operation to selectively whiten the domaindependent styles. We also tackle the lack of multicentre

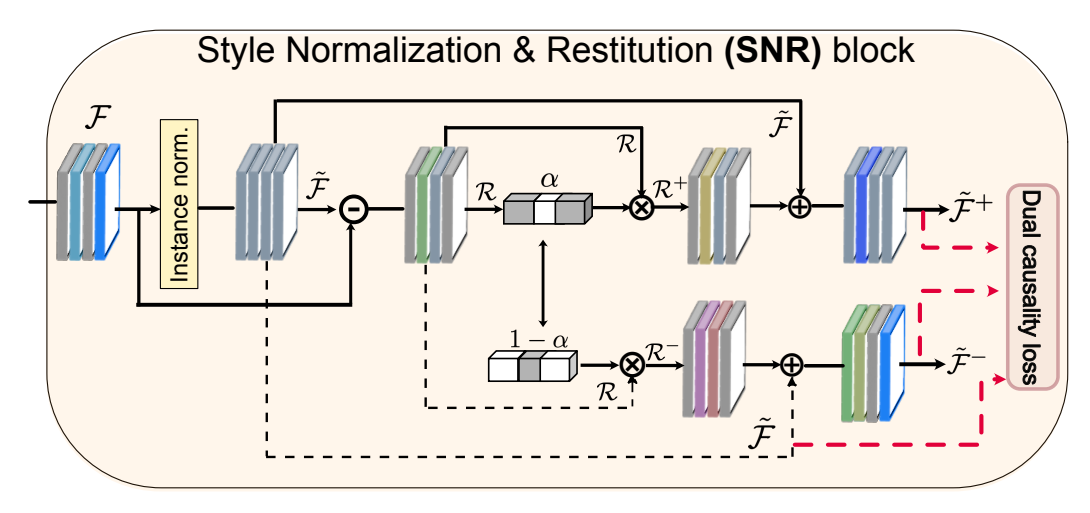


**Figure 5:** Features from intermediate backbone layers are fed to the SNR block. SNR applies instance normalization (IN) on input features, followed by channel attention to restore lost information due to IN. Dual causality loss encourages the disentanglement between useful and contaminated features.

annotated datasets by introducing HeiCholeSeg, a twocentre annotated dataset to evaluate the generalisability of models.

# 3.3. Style Normalization and Restitution (SNR block)

Several previous works (Pan et al., 2018; Li et al., 2017) have shown that instance normalization is less sensitive to style variations. Most of the earlier DG methods have used IN alongwith feature statistics (e.g. mean, variance, covariance) to extract the style information aiming to suppress domain-dependent styles and preserve the content for better generalisability. The problem with IN is that it lacks task awareness and results in the loss of discriminant information necessary for better performance Li et al. (2017). To tackle this problem, we incorporate the Style Normalization and Restitution (SNR) block which aims to restore the lost information due to IN by applying channel attention. Channel attention aims to decouple the task-relevant and nonrelevant features on channel dimensions to be consistent with the IN which also works on the feature channels. In the SNR block, features are first instance normalised, followed by a feature restoration process where the task-relevant and non-relevant features are distilled through channel attention.

Fig. 5 shows the overall flowchart of the SNR block originally proposed in (Jin et al., 2021). The SNR layer receives an input feature map  $\mathcal{F} \in \mathbb{R}^{N \times C \times H \times W}$  and outputs an enhanced map  $\widetilde{\mathcal{F}}^+ \in \mathbb{R}^{N \times C \times H \times W}$ . Instance normalization is first applied to eliminate style discrepancies in the features maps. It is followed by a restitution step where the task-specific features from the residual are restored (i.e., the difference between style normalised  $\widetilde{\mathcal{F}}$  and original feature  $\mathcal{F}$  maps). This restoration is carried out by masking  $\mathcal{R}$  with the channel attention vector  $\boldsymbol{\alpha} = [\alpha_1, \alpha_2, ... \alpha_C] \in \mathbb{R}^C$ . This masking operation is implemented using spatial global average pooling and two fully-connected (FC) layers.

Applying channel attention, we get,

$$\mathcal{R}^{+}(:,:,:,i) = \alpha_{i}\mathcal{R}(:,:,:,i)$$
 (1)

$$\mathcal{R}^{-}(:,:,:,i) = (1 - \alpha_i)\mathcal{R}(:,:,:,i)$$
 (2)

where  $\mathcal{R}(:,:,:,i)$  represents the  $i^{th}$  channel of the feature map  $\mathcal{R}$ . On the other side of Eqs., (1) and (2),  $\mathcal{R}^+$  and  $\mathcal{R}^-$  denote the task-relevant and irrelevant features, respectively. Enhanced  $(\widetilde{\mathcal{F}}^+)$  and corrupted feature maps  $(\widetilde{\mathcal{F}}^-)$  are then obtained by adding  $\mathcal{R}^+$  and  $\mathcal{R}^-$  to normalised features  $\widetilde{\mathcal{F}}$ , respectively. We integrate dual causality loss  $\mathcal{L}_{dc}$  function which is basically an entropy minimization loss constraint to enhance the disentanglement of task relevant and non-relevant features.

With the addition of  $\mathcal{R}^+$  to  $\widetilde{\mathcal{F}}$ , enhanced feature map  $\widetilde{\mathcal{F}}^+$  becomes more discriminative resulting in smaller entropy (pixel randomness or uncertainty), in contrast to the corrupted feature maps which have larger entropy. Dual Causality loss aims to enhance the separation between enhanced and corrupted features. In  $\mathcal{L}_{dc}$ , first we compute pixel-wise entropy with the function  $\mathcal{E}(.) = -p(.)\log p$ , where p is denotes softmax probability. The  $\mathcal{L}_{dc}$  consists of  $\mathcal{L}_{SNR}^+$  and  $\mathcal{L}_{SNR}^-$  i.e.,  $\mathcal{L}_{SNR}^+ + \mathcal{L}_{SNR}^-$ ,

$$\mathcal{L}_{SNR}^{+} = \text{Marginloss} \left( \frac{1}{w \times h} \sum_{j=1}^{h} \sum_{k=1}^{w} \mathcal{E} \left( \phi(\widetilde{\mathcal{F}}^{+}(j, k, :)) - \phi(\widetilde{\mathcal{F}}(j, k, :)) \right) \right)$$
(3)

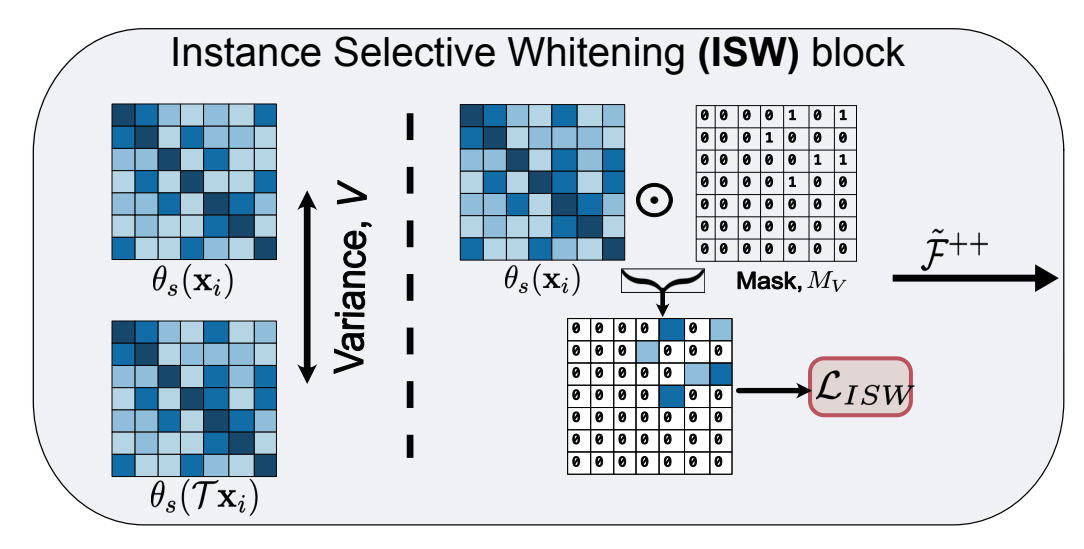


**Figure 6:** Instance selective whitening takes enhanced features from the SNR to selectively suppress the style-encoded information through instance selective whitening loss.

$$\begin{split} \mathcal{L}_{SNR}^{-} &= \mathrm{Marginloss}\Bigg(\frac{1}{w \times h} \sum_{j=1}^{h} \sum_{k=1}^{w} \\ &\mathcal{E}\left(\phi(\widetilde{\mathcal{F}}(j,k,:)) - \phi(\widetilde{\mathcal{F}}^{-}(j,k,:))\right)\Bigg) \end{split} \tag{4}$$

where  $\phi$  denotes softmax function and w, h represent height and width of feature vector containing probability values. On the other hand, Marginloss is  $\ln(1 + exp(.))$  represents a monotonically increasing function whose aim is to serve as smoother optimiser to avoid negative loss values.

# 3.4. Instance Selective Whitening (ISW block)

It has been shown that the whitening transformation (WT) can remove domain-specific information and improve the overall DG performance (Cho et al., 2019; Li et al., 2017; Pan et al., 2019). For a feature map  $\mathcal{F} \in \mathbb{R}^{N \times C \times H \times W}$ , WT is a linear transformation which standardises features by de-correlating the channels. It performs this de-correlation by making the feature covariance matrix  $(\theta_s)$  close to an identity matrix. The conventional way of computing WT through eigen value decomposition is highly computationally expensive. Thus an alternative implementation proposed in GDWCT (Cho et al., 2019) is implemented that computes the deep whitening transformation (DWT):

$$\mathcal{L}_{\text{DWT}} = \mathbb{E}[\|\theta_{u} - \mathbf{I}\|_{1}] \tag{5}$$

where E denotes the arithmetic mean.

The major limitation of WT is that it can distort the object boundaries (Li et al., 2017) or reduce feature discrimination (Pan et al., 2019) because  $\theta_s$  contains both style and content information. Therefore, in our framework we introduce the ISW block to selectively remove the style while retaining the structural information (see Figure 6).

Unlike prior approach (Choi et al., 2021) on DG, where feature whitening is applied directly on the instance normalised features, we pass the distilled features from the SNR block to the ISW block. The ISW block takes the enhanced features  $\tilde{\mathcal{F}}^+$  of the original and transformed images from the SNR block. The network is initially trained for n epochs (n was empirically set to 5) to obtain stable covariance matrices. Afterwards, the covariance  $\theta_s$  for both feature maps, as well as their variance V are computed as follows:

$$\theta_s = \frac{1}{h \times w} (\widetilde{\mathcal{F}}^+) (\widetilde{\mathcal{F}}^+)^T \tag{6}$$

$$V = \frac{1}{N} \sum_{i=1}^{N} \frac{1}{2} ((\theta_s(x_i) - \mu_\theta)^2 + (\theta_s(\mathcal{T}x_i) - \mu_\theta)^2)$$
 (7)

where  $\mu_{\theta}$  denotes the mean of both covariance matrices. It is assumed that high variance values in V indicate the presence of style information which must be suppressed. Therefore, a mechanism to disentangle and separate such values was implemented using k-means clustering. This results in two distinct groups,  $G_{high}$  (containing domain style) and  $G_{low}$  (containing content information). Based on this clustered V, we compute the mask  $M_v$  and consequently  $\mathcal{L}_{ISW}$  as follows,

$$\mathcal{L}_{ISW} = \mathbb{E}[|\theta_s \bigcirc \mathcal{M}_v|] \tag{8}$$

The overall cost function for our proposed approach is given by,

$$\mathcal{L}_{total} = \mathcal{L}_{task} + \sum_{i}^{L} \lambda_1 \mathcal{L}_{ISW}^{i} + \lambda_2 \mathcal{L}_{dc}^{i}$$
 (9)

with  $\lambda_1$  and  $\lambda_2$  denote the weight of the ISW and DC losses, respectively, L represents the number of layers and  $\mathcal{L}_{task}$  is cross-entropy loss for semantic segmentation.

Table 2 Table showing mean Intersection over Union (mIoU), Dice, Precision, Recall and accuracy scores for the SOTA and our proposed method on CholecSeg8K and HeiCholeSeg datasets. The best and second best results are bolded and underlined,

| In-domain distribution       |   | Ch                                      | olecSeg8K Test                          | set                                     |   |
|------------------------------|---|---|---|---|---|
| Method                       | mean IoU                                | mean DSC                                | Precision                               | Recall                                  | Pixel Accuracy                          |
| Baseline Chen et al. (2018)  | $87.67 \pm 0.624$                       | $92.45 \pm 0.432$                       | $94.57 \pm 0.380$                       | $91.66 \pm 0.450$                       | $97.78 \pm 0.190$                       |
| IBN-Net Pan et al. (2018)    | $86.82 \pm 0.433$                       | $91.63 \pm 0.320$                       | $\overline{93.26} \pm \overline{0.290}$ | $92.00 \pm 0.330$                       | $97.76 \pm 0.160$                       |
| RobustNet Choi et al. (2021) | $87.67 \pm 0.566$                       | $92.52 \pm 0.411$                       | $93.25 \pm 0.370$                       | $92.31 \pm 0.390$                       | $97.85 \pm 0.170$                       |
| SNR Jin et al. (2021)        | $88.30 \pm 0.423$                       | $91.89 \pm 0.450$                       | $93.14 \pm 0.410$                       | $93.84 \pm 0.420$                       | $97.90 \pm 0.170$                       |
| SAN-SAW Peng et al. (2022)   | $82.54 \pm 0.462$                       | $89.88 \pm 0.476$                       | $91.69 \pm 0.450$                       | $88.64 \pm 0.480$                       | $96.16 \pm 0.210$                       |
| SHADE Zhao et al. (2022)     | $86.78 \pm 0.503$                       | $93.45 \pm 0.357$                       | $91.58 \pm 0.320$                       | $92.47 \pm 0.391$                       | $97.60 \pm 0.178$                       |
| SAMed Zhang and Liu (2023)   | $86.00 \pm 0.550$                       | $\overline{91.24 \pm 0.368}$            | $92.09 \pm 0.340$                       | $92.47 \pm 0.360$                       | $97.71 \pm 0.160$                       |
| BlindNet Ahn et al. (2024)   | $86.95 \pm 0.624$                       | $92.63 \pm 0.356$                       | $92.90 \pm 0.330$                       | $92.43 \pm 0.350$                       | $97.34 \pm 0.190$                       |
| RobustSurg (Ours)            | $89.32\pm0.376$                         | $\textbf{93.64} \pm \textbf{0.412}$     | $96.91\pm0.300$                         | $93.89 \pm 0.370$                       | $98.62 \pm 0.140$                       |
| Out-of-domain distribution   |   | Не                                      | iCholeSeg Cent                          | re 1                                    |   |
| Baseline Chen et al. (2018)  | $44.48 \pm 0.589$                       | $58.02 \pm 0.418$                       | $64.47 \pm 0.395$                       | $60.36 \pm 0.442$                       | $76.05 \pm 0.183$                       |
| IBN-Net Pan et al. (2018)    | $45.25 \pm 0.403$                       | $58.74 \pm 0.309$                       | $65.27 \pm 0.284$                       | $62.82 \pm 0.326$                       | $76.56 \pm 0.159$                       |
| RobustNet Choi et al. (2021) | $45.61 \pm 0.538$                       | $58.82 \pm 0.398$                       | $\overline{63.65} \pm \overline{0.363}$ | $62.02 \pm 0.381$                       | $75.78 \pm 0.169$                       |
| SNR Jin et al. (2021)        | $46.00 \pm 0.429$                       | $59.03 \pm 0.437$                       | $61.74 \pm 0.389$                       | $68.50 \pm 0.415$                       | $76.87 \pm 0.172$                       |
| SAN-SAW Peng et al. (2022)   | $39.34 \pm 0.487$                       | $51.96 \pm 0.466$                       | $62.61 \pm 0.452$                       | $56.65 \pm 0.436$                       | $67.52 \pm 0.208$                       |
| SHADE Zhao et al. (2022)     | $46.37 \pm 0.518$                       | $59.40 \pm 0.367$                       | $64.28 \pm 0.330$                       | $63.72 \pm 0.340$                       | $72.24 \pm 0.110$                       |
| SAMed Zhang and Liu (2023)   | $36.01 \pm 0.456$                       | $45.89 \pm 0.345$                       | $46.83 \pm 0.331$                       | $51.45 \pm 0.362$                       | $56.12 \pm 0.165$                       |
| BlindNet Ahn et al. (2024)   | $46.16 \pm 0.603$                       | $59.40 \pm 0.339$                       | $64.51 \pm 0.315$                       | $67.78 \pm 0.344$                       | $76.98 \pm 0.189$                       |
| RobustSurg (Ours)            | $48.55 \pm 0.352$                       | $61.35 \pm 0.401$                       | $65.49 \pm 0.289$                       | $73.78 \pm 0.363$                       | $81.10 \pm 0.138$                       |
| Out-of-domain distribution   |   | He                                      | iCholeSeg Cent                          | re 2                                    |   |
| Baseline Chen et al. (2018)  | $40.96 \pm 0.578$                       | $55.50 \pm 0.389$                       | $56.24 \pm 0.371$                       | $74.15 \pm 0.441$                       | $67.20 \pm 0.183$                       |
| IBN-Net Pan et al. (2018)    | $44.46 \pm 0.412$                       | $58.52 \pm 0.344$                       | $61.01 \pm 0.331$                       | $74.40 \pm 0.360$                       | $69.30 \pm 0.157$                       |
| RobustNet Choi et al. (2021) | $45.63 \pm 0.498$                       | $59.71 \pm 0.381$                       | $61.30 \pm 0.352$                       | $\overline{73.49} \pm \overline{0.377}$ | $67.75 \pm 0.172$                       |
| SNR Jin et al. (2021)        | $\overline{43.98} \pm \overline{0.395}$ | $\overline{58.55} \pm \overline{0.402}$ | $59.81 \pm 0.375$                       | $74.19 \pm 0.391$                       | $75.67 \pm 0.169$                       |
| SAN-SAW Peng et al. (2022)   | $44.93 \pm 0.439$                       | $58.83 \pm 0.417$                       | $65.31 \pm 0.305$                       | $61.33 \pm 0.357$                       | $68.73 \pm 0.210$                       |
| SHADE Zhao et al. (2022)     | $44.73 \pm 0.480$                       | $59.32 \pm 0.320$                       | $\overline{56.43} \pm \overline{0.340}$ | $73.20 \pm 0.380$                       | $65.36 \pm 0.150$                       |
| SAMed Zhang and Liu (2023)   | $38.11 \pm 0.461$                       | $47.44 \pm 0.358$                       | $51.72 \pm 0.336$                       | $51.79 \pm 0.369$                       | $59.22 \pm 0.162$                       |
| BlindNet Ahn et al. (2024)   | $43.92 \pm 0.567$                       | $58.15 \pm 0.366$                       | $61.93 \pm 0.341$                       | $70.57 \pm 0.359$                       | $75.77 \pm 0.186$                       |
| RobustSurg (Ours)            | $50.40\pm0.341$                         | $64.25 \pm 0.378$                       | $66.95 \pm 0.297$                       | $73.62 \pm 0.354$                       | $\overline{76.15} \pm \overline{0.138}$ |

#### 4. Implementation details

The proposed method was implemented using the Py-Torch framework. All the experiments were conducted using 2 NVIDIA Tesla P100-SXM2-16GB GPUs. The model was trained until convergence was reached as per the early stopping criteria. The SGD optimiser and starting learning rate of  $1e^{-2}$  and momentum of 0.9 with polynomial learning rate scheduling with power of 0.9 was used for loss minimization. We also use various augmentations such as color jittering, Gaussian blur, random cropping, random horizontal flipping and random scaling.

# 4.1. Training and test setup

We conducted experiments on three different dataset settings to validate the model performance on both indomain and out-of-domain distributions. In the first setup, we used the publicly available CholecSeg8K (Hong et al., 2020) for training and in-domain testing and our newly introduced HeiCholeSeg cnter 1 and 2 for evaluation. We randomly split CholecSeg8k dataset into 80%, 10%, 10%

for training, validation and test, respectively. For unseen centre generalisability test, we used all the annotated images from both centres of HeiCholeSseg centre. In the second setup, we used the EndoUDA dataset for validating the modality-agnostic performance of our model. We use the standard splits for training, validation and testing reported in Celik et al. (2021) for both the wite light imaging (WLI) and narrow-band imaging (NBI) modalities. In the third setup, we train our model using standard train-val-test splits of publicly available cataract surgery dataset (CaDIS) and for OOD testing, we used cataract-1K dataset which was recorded at a different hospital.

#### 4.2. Evaluation metrics

Widely used intersection-over-union (IoU =  $\frac{TP}{TP+FP+FN}$ ), dice similarity coefficient (DSC =  $\frac{2TP}{2TP+FP+FN}$ ), mean pixel accuracy (Pixel Accuracy =  $\frac{TP}{TP+TN}$ ), precision (Prec. =  $\frac{TP}{TP+FP}$ ) and recall (Rec. =  $\frac{TP}{TP+FN}$ ) have been used for comparing the segmentation results of the

tested models. Here TP, TN, FP, FN represent true positive, true negative, false positive, false negative respectively.

# 4.3. Comparison with state-of-the-art methods

DeepLabv3+ (Chen et al., 2018) with ResNet50 backbone is established as the baseline method in our work. We use subsequent SOTA methods addressing the problem of model generalisability. For instance, we compare with IBN-Net which introduced the idea of instance normalization followed by RobustNet which combined the instance norm with instance whitening. We also carried out a comparison with the style restitution method called SNR, and other instance norm based methods such as SAN-SAW and Blind-Net which utilise class-wise distributed alignment in the segmentation decoder. Style diversification being a strong approach in DG, we also include comparison with SHADE which proposed style-diversified samples. Finally, we include an SAM-based method to evaluate its performance in the endoscopic domain.

### 5. Results and discussion

In this Section, we comprehensively present results on different IID and OOD data settings. As our main focus is developing generalisable models on surgical dataset settings, we first discuss quantitative results on both IID and OOD settings in Section 5.1. Section 5.2 provides the results on individual classes for both IID and OOD datasets. Qualitative results on presented in Section 5.3. Afterwards, we discuss ablation experiments by taking CholecSeg8K dataset validation set in Section 5.6. In the preceding Section 5.7, we provide additional experimental results on two other dataset settings, one with cross-centre cataract surgery dataset (CaDIS and Cataract-1K), and one with cross-domain endoscopic dataset (EndoUDA).

#### 5.1. Quantitative results

In-domain distribution: Table 2 shows that our method (RobustSurg) achieves SOTA performance on the in-domain CholecSeg test set on all evaluation metric. Specifically, it achieves the highest mean IoU of 89.32 surpassing the the baseline by almost 2% and the second best method by 1.2% on mean IoU score. RobustSurg also outperforms other methods on Dice similarity coefficient, for example achieves 1.2% higher mean DSC as compared to the baseline. Apart from the overlap, it is also important to reduce false positive rate. Therefore, in terms of precision and recall, RobustSurg achieves 2.5% higher precision than the second best method which is baseline, and outperforms all other methods on recall score by 1-2% except SNR which performs almost equally well. Similar trends can be observed on pixel-level performance where RobustSurg gets approximately 1% higher pixel accuracy as compared to other methods.

# **Out-of-the domain distribution:**

To evaluate the robustness and generalisability of segmentation models, we tested on the HeiCholeSeg dataset from two independent clinical centres. As shown in Table 2, our

proposed method, RobustSurg, significantly outperforms all competing methods across both domains. On HeiCholeSeg centre 1, RobustSurg achieves the highest mean IoU 48.55 which is 9.17% higher than the baseline and 4.7% than the SHADE which is the second best method. Similarly, our method produces a Dice score of 61.35 which is 5.73% and 3.28% higher than the baseline and SHADE. Similar trends can be observed on other evaluation metrics. Our method achieves even higher metrics on centre 2 data where it outperforms baseline by 23.04% IoU score and the second best method RobustNet by 10.45%. It also achieves 15.76% and 7.60% higher Dice score against baseline and second best method. RobustSUrg achieves consistently higher performance on other evaluation metrics compared to all the SOTA methods.

# 5.2. Class-wise performance

We also report mean pixel accuracies and IoU scores (Table 4) on every semantic class on both CholecSeg8k IID and OOD HeiCholeSeg centres 1 and 2. Our method achieved higher pixel accuracy showing robust performance. On IID, the results indicate that our method performs well on most classes, for instance, our method produces higher IoU score on all the classes except blood, hepatic vein, gallbladder and liver ligament where it shows competitive performance. On HeiCholeSeg center 1, RobustSurg produces higher IoU score on liver (69.32 against the second best 64.45 on RobustNet), grasper instrument (60.23 against the second best 59.86 on RobustNet), and Abdominal wall (68.42 against second best 64.54 on abdominal wall). RobustSurg also produces the second best performance on hook instrument (27.36 against best 29.03 on SHADE), and perform competitively on Gallbladder class (48.20 against the best 50.59 on IBN-Net). Similarly on center 2, RobustSurg achieves 6.7% higher IoU on liver, 4% higher IoU on GI tract, and 23.2% IoU on abdominal wall classes against the second best methods. Further, RobustSurg performance remains the second best on background class and competitive on fat and gallbladder classes.

# 5.3. Qualitative results

Fig. 7 presents the qualitative results on both in-domain distribution (row 1), OOD centre 1 (row 2) and OOD centre 2 (row 3). In the in-domain dataset, most of the methods are able to distinguish classes correctly; however, the accuracy of segmentation varies. For instance, the grasper instrument on top is more precisely segmented by our method, where other methods struggle to correctly segment it. In the unseen dataset HeiChole (row 2), methods struggle to distinguish between grasper and hook instrument classes due to the vendor differences between instrument types between training and testing domains. IBN-Net suffers from oversegmentation in the grasper instrument class. In the centre 2 (row 3), most methods struggle on one leg of grasper, and the part above the instrument is misclassified, but our method segments the semantic classes more accurately.

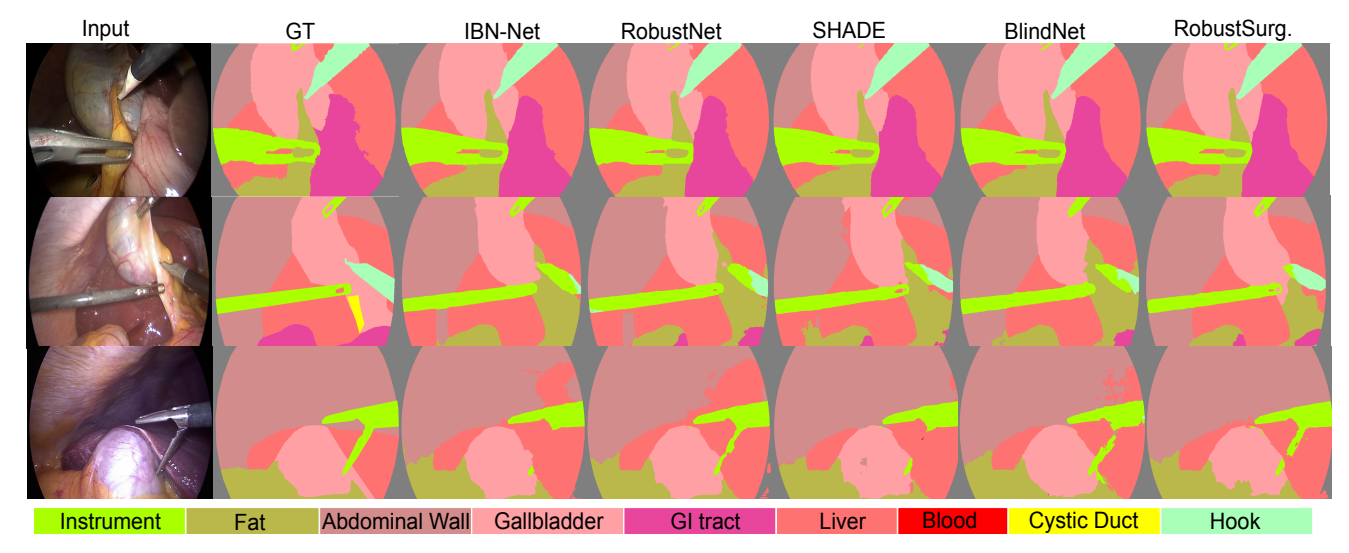


Figure 7: Qualitative results. Top row rows contain qualitative performance on IID CholecSeg8k and bottom two rows show OOD HeiCholeSeg datasets on centre 1 and centre 2, respectively.

# **5.4.** Statistical analysis

Fig. 8 demonstrates the paired t-test analyses between RobustSurg and other methods on both in-domain and outof-domain datasets. It can be observed that RobustSurg shows highly significant difference compared to all other methods on all datasets, except with RobustNet on Hei-CholeSeg centre 1, where p-value is borderline. Robust-Surg also exhibited smaller standard deviation compared to most of the methods, as reflected by narrower interquartile (IQRs). On the CholecSeg data, RobustSurg shows a very narrow deviation as compared to SAMed and SAN-SAW and a competitive performance with other methods. Similarly, on both HeiCholeSeg centres, our method acheives smaller deviation and higher median values as compared to all other methods. These results highlight RobustSurg's robustness to institutional variability and imaging conditions differences, with statistical significance reached in the vast majority of pairwise comparisons.

#### 5.5. Computational cost analysis

Table 3 shows the comparison of computational cost analysis of our method and the state-of-the-art. We report this cost analysis in terms of number of parameters, GFLOPS, and inference time. We can observe that when compared with similar other models such as DeepLabv3+, IBN-Net, RobustNet, and SNR, our method brings a small increase in model size and computational complexity. For example RobustSurg only brings an increase of 1.5% in model size (45.785M vs. 45.077M), and 0.02% increase in the computational complexity (436.83 vs. 436.70) and a 5.12% slower inference as compared to the DeepLabv3+ baseline.

# 5.6. Ablation study

In this section, we present different ablation experiments to demonstrate the effectiveness of adding individual components into our proposed RobustSurg method.

Impact of different backbones. To validate the wide applicability of RobustSurg, we conducted experiments with two other backbone networks, MobileNetv2 and ShuffleNetv2. Table 5 shows the results on both in-domain and out-of-domain datasets. Our method shows better performance with both backbones as compared to RobustNet, IBN-Net and baseline with both backbones. This shows that our domain-invariant learning pipeline is backbone-agnostic and can be used with variety of backbone architectures.

Design choices of whitening and restitution blocks. Table 6 ablates different network configurations where we restrict ISW to first three layers since deeper layers are not rich in style information and RobustNet has shown the best performance on these layers. Afterwards, we change SNR between the residual layers and see how the network behaves. It can be observed that the proposed SRW block (ISW and SNR) configured between layer 1 to layer 3 of ResNet50 produces the best performance.

Separating covariance elements. We adopt k-means clustering approach to separate the covariance elements into two groups, i.e., domain-dependent styles and domain-invariant content based on the variance of covariance elements of original and photometric transformed images. As discussed in Section 3.4, we divide the variance elements into k clusters based on variance magnitude. The first m elements represent domain-invariant content (low variance) and the remaining elements are considered sensitive to photometric transformation meaning they represent the domain-specific styles. Table 7 shows that the optimal k value is 2.

Effectiveness of dual causality loss. Table 8 shows the ablation experiments on the dual causality loss constraint. We observe that inclusion of the dual causality loss produces the best performance on both IID and OOD data. The addition of  $\mathcal{L}_{dc}$  surpassed the architecture without it by approximately 2% on IID data and 1.5% on OOD data. The dual causality loss enhances the process of disentanglement

**Table 3**Comparison of computational cost. All the models were tested with an image of size 480×860 on NVIDIA Tesla P100-SXM2-16GB GPU. The inference time was averaged over all the validation set.

| Method                        | # of Params | GFLOPs | Inference Time (ms) |
|-------------------------------|-------------|--------|---------------------|
| DeepLabv3+ Chen et al. (2018) | 45.077M     | 436.70 | 11.7                |
| IBN-Net Pan et al. (2018)     | 45.079M     | 436.84 | 11.9                |
| RobustNet Choi et al. (2021)  | 45.077M     | 436.81 | 11.9                |
| SNR Jin et al. (2021)         | 46.068M     | 459.12 | 13.1                |
| SAN-SAW Peng et al. (2022)    | 25.069M     | 655.25 | 16.1                |
| SHADE Zhao et al. (2022)      | 45.077M     | 436.70 | 34.7                |
| SAMed Zhang and Liu (2023)    | 639.18M     | 5490   | 122.5               |
| BlindNet Ahn et al. (2024)    | 50.100M     | 218.40 | 11.2                |
| RobustSurg                    | 45.785M     | 436.83 | 12.3                |

**Table 4**Quantitative results for pixel accuracy and IoU for each semantic class. The models are trained on CholecSeg and tested on in-domain CholecSeg test set and HeiCholeSeg Centre 1 and Centre 2 using a ResNet50 backbone. The best and second best results are **bolded** and <u>underlined</u>, respectively.

| Methods                      | Pixel<br>Accuracy | mloU  | Background | Liver | GI tract | Fat   | Grasper | Connective tissue | Abdominal Wall | Blood | Cystic Duct | Hook  | Hepatic Vein | Gallbladder | Liver Ligament |
|------------------------------|-------------------|-------|------------|-------|----------|-------|---------|-------------------|----------------|-------|-------------|-------|--------------|-------------|----------------|
| Baseline Chen et al. (2018)  | 97.78             | 87.67 | 98.52      | 94.92 | 88.82    | 94.80 | 89.46   | 88.70             | 97.44          | 75.21 | 75.42       | 91.80 | 55.91        | 93.12       | 95.59          |
| IBN-Net Pan et al. (2018)    | 97.76             | 86.82 | 98.82      | 94.92 | 87.18    | 94.45 | 88.43   | 88.77             | 97.45          | 74.31 | 71.33       | 91.67 | 51.76        | 92.76       | 96.82          |
| RobustNet Choi et al. (2021) | 97.85             | 87.67 | 98.70      | 95.12 | 90.21    | 94.72 | 89.38   | 89.34             | 97.40          | 73.87 | 72.36       | 92.36 | 55.32        | 93.76       | 97.84          |
| SNR Jin et al. (2021)        | 97.90             | 88.30 | 99.01      | 95.15 | 88.82    | 94.65 | 89.54   | 88.75             | 97.60          | 76.88 | 78.09       | 92.45 | 56.57        | 93.28       | 97.42          |
| SAN-SAW Peng et al. (2022)   | 96.16             | 82.54 | 98.95      | 91.96 | 83.69    | 92.04 | 82.75   | 78.09             | 93.12          | 63.80 | 70.77       | 86.58 | 53.51        | 85.79       | 91.97          |
| SHADE Zhao et al. (2022)     | 97.60             | 86.78 | 97.90      | 94.50 | 87.40    | 94.60 | 88.00   | 88.60             | 97.30          | 71.40 | 72.40       | 90.30 | 58.50        | 93.00       | 94.30          |
| SAMed Zhang and Liu (2023)   | 97.71             | 86.00 | 96.14      | 93.57 | 84.48    | 92.37 | 80.36   | 88.94             | 93.80          | 67.01 | 76.43       | 89.25 | 68.54        | 92.40       | 94.73          |
| BlindNet Ahn et al. (2024)   | 97.34             | 86.42 | 98.04      | 94.33 | 87.44    | 94.57 | 87.29   | 88.14             | 96.98          | 71.16 | 72.12       | 90.15 | 55.60        | 92.48       | 95.15          |
| RobustSurg. (ours)           | 98.62             | 89.32 | 99.42      | 97.83 | 92.52    | 95.32 | 91.97   | 91.32             | 98.36          | 75.95 | 79.82       | 92.46 | 62.31        | 92.92       | 97.79          |
| HeiCholeSeg Centre 1         |                   |       |            |       |          |       |         |                   |                |       |             |       |              |             |                |
| Baseline Chen et al. (2018)  | 76.05             | 44.48 | 82.10      | 63.27 | 17.73    | 15.59 | 51.93   | -                 | 58.92          | -     | -           | 20.39 | -            | 45.98       | -              |
| IBN-Net Pan et al. (2018)    | 76.56             | 45.25 | 85.70      | 63.52 | 21.52    | 14.79 | 54.26   | -                 | 52.06          | -     | -           | 19.58 | -            | 50.59       | -              |
| RobustNet Choi et al. (2021) | 75.78             | 45.61 | 83.88      | 64.45 | 16.42    | 13.16 | 59.86   | -                 | 60.01          | -     | -           | 26.22 | -            | 40.94       | -              |
| SNR Jin et al. (2021)        | 76.87             | 46.00 | 93.91      | 58.22 | 53.63    | 35.25 | 50.36   | -                 | 34.50          | -     | -           | 23.40 | -            | 18.79       | -              |
| SAN-SAW Peng et al. (2022)   | 67.52             | 39.34 | 87.67      | 54.22 | 11.57    | 9.65  | 55.02   | _                 | 44.59          | -     | -           | 17.00 | -            | 35.00       | -              |
| SHADE Zhao et al. (2022)     | 72.24             | 46.37 | 85.40      | 61.23 | 15.01    | 13.23 | 58.02   | _                 | 64.54          | -     | -           | 29.03 | -            | 44.52       | _              |
| SAMed Zhang and Liu (2023)   | 56.12             | 36.01 | 64.24      | 61.16 | 14.00    | 9.13  | 34.26   | _                 | 45.25          | -     | -           | 10.40 | -            | 49.62       | _              |
| BlindNet Ahn et al. (2024)   | 76.98             | 46.16 | 84.39      | 63.03 | 19.00    | 10.95 | 59.29   | _                 | 58.51          | -     | -           | 26.42 | -            | 47.76       | _              |
| RobustSurg. (ours)           | 81.10             | 48.55 | 84.79      | 69.32 | 20.57    | 10.95 | 60.23   | -                 | 68.42          | -     | -           | 27.36 | -            | 47.38       | -              |
| HeiCholeSeg Centre 2         |                   |       |            |       |          |       |         |                   |                |       |             |       |              |             |                |
| Baseline Chen et al. (2018)  | 67.20             | 44.48 | 87.89      | 52.54 | 34.35    | 37.93 | 44.09   | -                 | 27.13          | -     | -           | 17.90 | -            | 25.92       | -              |
| IBN-Net Pan et al. (2018)    | 69.30             | 44.46 | 93.47      | 61.58 | 49.18    | 36.28 | 42.68   | -                 | 29.30          | -     | -           | 23.75 | -            | 19.49       | -              |
| RobustNet Choi et al. (2021) | 67.75             | 45.63 | 93.69      | 56.12 | 52.60    | 34.70 | 50.95   | -                 | 29.00          | -     | -           | 27.60 | -            | 20.39       |                |
| SNR Jin et al. (2021)        | 75.67             | 43.98 | 91.16      | 56.71 | 39.88    | 35.80 | 49.17   | -                 | 27.21          | -     | -           | 29.23 | -            | 22.73       | -              |
| SAN-SAW Peng et al. (2022)   | 68.73             | 44.93 | 96.88      | 61.09 | 22.71    | 32.56 | 52.89   | -                 | 39.82          | -     | -           | 30.53 | -            | 22.94       | _              |
| SHADE Zhao et al. (2022)     | 65.36             | 44.73 | 91.50      | 51.60 | 32.50    | 34.20 | 56.70   | -                 | 36.40          | -     | -           | 20.10 | -            | 34.90       | _              |
| SAMed Zhang and Liu (2023)   | 59.22             | 38.11 | 75.96      | 62.40 | 14.43    | 25.23 | 33.25   | -                 | 41.53          | -     | -           | 16.94 | -            | 35.14       | _              |
| BlindNet Ahn et al. (2024)   | 75.77             | 43.92 | 92.96      | 63.86 | 31.58    | 31.33 | 46.27   | -                 | 34.93          | -     | -           | 29.70 | -            | 20.78       | -              |
| RobustSurg. (ours)           | 76.15             | 50.40 | 96.33      | 68.13 | 54.63    | 31.99 | 49.45   | _                 | 51.17          | -     | -           | 23.63 | -            | 27.92       | -              |

of relevant and non-relevant features. Furthermore, the addition of individual loss components ( $\mathcal{L}_{SNR}^+$  and  $\mathcal{L}_{SNR}^-$ ) shows that skipping the contaminated features from the overall loss constraint degrades the performance.

**Feature-map visualization.** Fig. 9 presents the feature maps obtained from third SNR block (i.e., SNR-3) on the EndoUDA polyp dataset to understand the effectiveness of SNR block. We obtained individual feature maps by summarizing the map on channel dimension followed by  $\ell_2$ 

normalization. Fig. 9 depicts the original normalised feature map, enhanced features and the contaminated feature map. We can see that addition of the task-relevant feature enhances the model's ability to focus on discriminative areas of the image such as anatomical regions, instruments etc, while addition of task-irrelevant features does not have a uniform response on the discriminative areas.

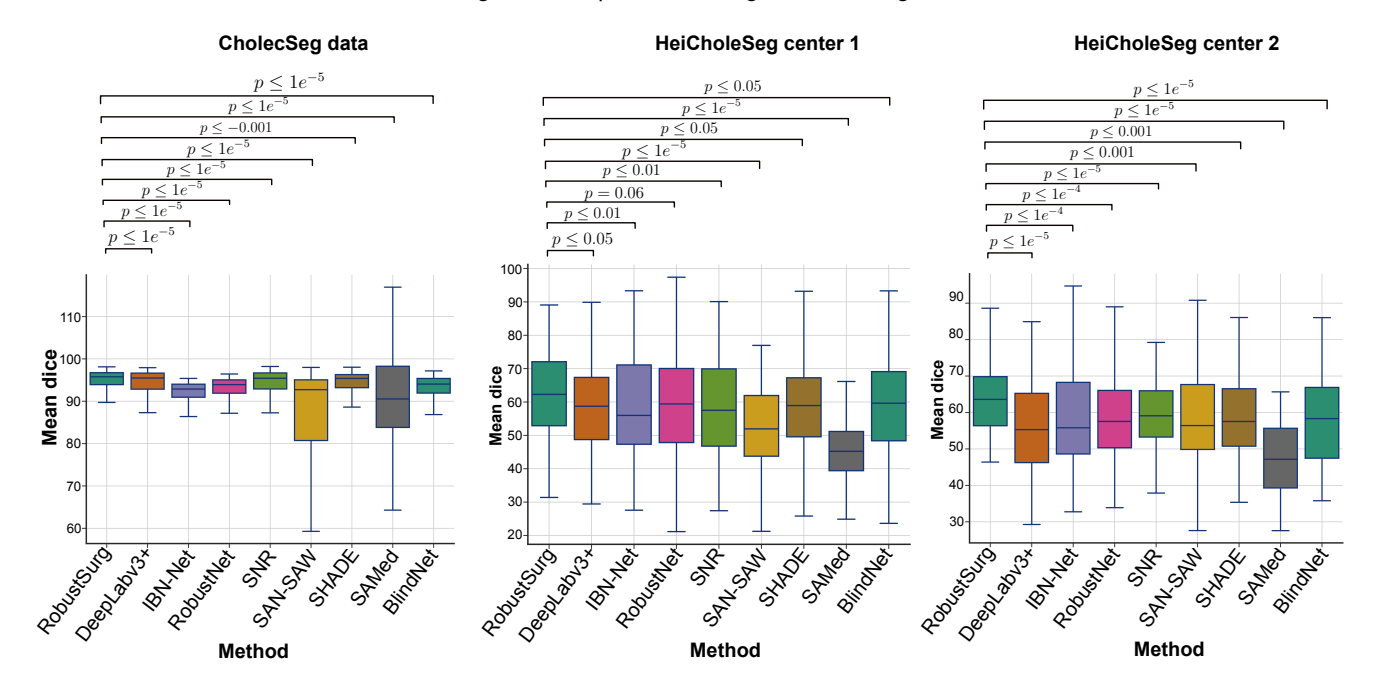


Figure 8: Box-plots for paired t-test on in-domain CholecSeg dataset and OOD HeiCholecSeg centre 1 and centre 2 datasets.

**Table 5**Comparison of IoU and Dice scores for different methods under MobileNet and ShuffleNet backbones across three datasets. The best and second best results are **bolded** and underlined, respectively.

| Backbone     | Method                       |       | Seg8K |       | leSeg-C1 |       | leSeg-C2 |
|--------------|------------------------------|-------|-------|-------|----------|-------|----------|
|              |                              | loU   | Dice  | loU   | Dice     | loU   | Dice     |
|              | Baseline Chen et al. (2018)  | 87.12 | 92.64 | 44.71 | 58.13    | 34.46 | 50.37    |
| MobileNetv2  | IBN-Net Pan et al. (2018)    | 87.32 | 92.81 | 44.63 | 57.56    | 45.12 | 59.15    |
|              | RobustNet Choi et al. (2021) | 85.73 | 91.71 | 44.88 | 58.10    | 42.78 | 57.55    |
|              | RobustSurg (Ours)            | 87.95 | 92.88 | 47.91 | 61.15    | 50.11 | 63.99    |
|              | Baseline Chen et al. (2018)  | 86.41 | 92.19 | 44.25 | 57.25    | 44.71 | 58.76    |
| ShuffleNetv2 | IBN-Net Pan et al. (2018)    | 86.80 | 92.50 | 45.85 | 58.50    | 45.05 | 59.18    |
|              | RobustNet Choi et al. (2021) | 86.98 | 92.77 | 44.20 | 57.27    | 46.87 | 61.01    |
|              | RobustSurg (Ours)            | 87.52 | 93.20 | 48.21 | 61.20    | 50.25 | 64.01    |

Comparison of covariance matrices. To demonstrate the enhanced feature whitening operation offered by our approach, we present different covariance matrices of intermediate feature maps of IBN-Net, RobustNet and our

RobustSurg. As shown in Fig. 10, the first row represents covariance matric for first convolutional layer, and second and third rows represent the covariance matrices for second and third convolutional layers respectively. As pointed out

**Table 6**Effect of using single or multiple SNR blocks with fixed ISW blocks. Layers 1 to 5 represent ResNet-50 layers. Best values are represented in **Bold** and second best <u>underlined</u>.

| ISW              |       |       |       |       |                  |       |       |       |       |                   |
|------------------|-------|-------|-------|-------|------------------|-------|-------|-------|-------|-------------------|
| $\overline{L_1}$ | $L_2$ | $L_3$ | $L_4$ | $L_5$ | $\overline{L_1}$ | $L_2$ | $L_3$ | $L_4$ | $L_5$ | Validation (IID)) |
| <b>√</b>         | 1     | 1     | Х     | Х     | Х                | 1     | Х     | Х     | Х     | 87.82             |
| ✓                | ✓     | ✓     | Х     | Х     | Х                | ✓     | ✓     | X     | X     | 88.12             |
| 1                | ✓     | ✓     | Х     | Х     | Х                | ✓     | ✓     | ✓     | X     | 88.92             |
| /                | ✓     | 1     | X     | X     | X                | Х     | ✓     | 1     | X     | 87.54             |
| ✓                | ✓     | ✓     | X     | X     | X                | X     | ✓     | X     | ✓     | 87.68             |

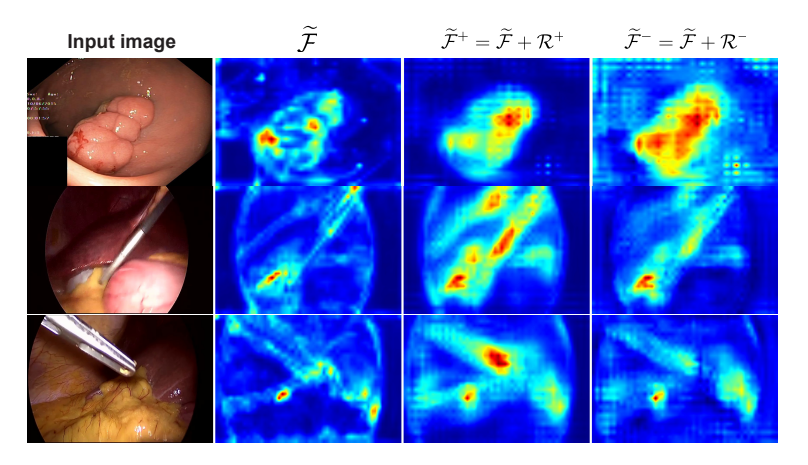


**Figure 9:** Activation feature maps from the third SNR block: The activation feature maps show that the model can disentangle task-relevant features from the irrelevant features using the residual feature  $R^+$ .

**Table 7**Effect of k value on model performance. Best values are represented in **Bold** and second best underlined.

|                   | Validation (IID) |       |       |              |  |  |  |  |
|-------------------|------------------|-------|-------|--------------|--|--|--|--|
| Method            | mloU             | Prec. | Rec.  | Acc.         |  |  |  |  |
| DeepLabv3+        | 87.40            | 92.67 | 92.90 | 90.73        |  |  |  |  |
| RobustSurg (k=2)  | 88.92            | 94.61 | 94.66 | 91.96        |  |  |  |  |
| RobustSurg (k=3)  | 88.49            | 94.31 | 94.44 | 91.66        |  |  |  |  |
| RobustSurg (k=5)  | 88.49            | 93.37 | 92.13 | 91.66        |  |  |  |  |
| RobustSurg (k=7)  | 88.38            | 93.50 | 94.17 | 91.62        |  |  |  |  |
| RobustSurg (k=10) | 87.67            | 94.16 | 92.71 | 90.98        |  |  |  |  |
| RobustSurg (k=20) | 88.62            | 93.58 | 94.35 | <u>91.81</u> |  |  |  |  |

**Table 8** Effect of dual causality loss  $(\mathcal{L}_{dc} = \mathcal{L}_{SNR}^+ + \mathcal{L}_{SNR}^-)$ . Best values are represented in **Bold** and second best underlined.

|  |       | Validati | on (IID) |       |
|--|-------|----------|----------|-------|
| Method                                     | mloU  | Prec.    | Rec.     | Acc.  |
| DeepLabv3+                                 | 87.40 | 92.67    | 92.90    | 90.73 |
| RobustSurg (w/o $\mathcal{L}_{SNR}^+$ )    | 88.10 | 93.38    | 93.98    | 91.41 |
| RobustSurg (w/o $\mathcal{L}_{SNR}^{-1}$ ) | 87.77 | 94.21    | 91.52    | 90.32 |
| RobustSurg (w/o $\mathcal{L}_{dc}$ )       | 86.41 | 92.58    | 89.45    | 88.98 |
| RobustSurg (with $\mathcal{L}_{dc}$ )      | 88.92 | 94.61    | 94.66    | 91.96 |

by IBN-Net, the style information is encoded in the early layers of the network. We can observe that our method using enhanced features by restitution operation is capable of perming whitening operation to remove domain styles more effectively as compared to other two methods.

# 5.7. Generalisability tests on endoscopic and cataract surgery datasets.

**Results on EndoUDA** (polyp): Table 9 shows results on EndoUDA dataset. On EndoUDA polyp with IID, our proposed model got 81.67% mIoU score which is slightly higher than the baseline and SNR method and 5.9%, 4.4%, 2.9% and 4.4% higher as compared to IBN-Net, RobustNet,

SAMed, and BlindNet. On the OOD side, our model with 78.30% mIoU outperformed the baseline by 21.8% and other SOTA methods with a significant margin of 11.4% RobustNet, 15% IBN-Net, 5.6% SAMed, 9.7% SNR, and 46% BlindNet respectively. On the mDSC score, similar performance can be observed with our model outperforming the baseline by 22.11% and second best method SAMed by 8.3%.

Results on EndoUDA (BE): On EndoUDA (BE) IID, our model produced 91.50 mIoU and 95.01 mDSC score which is higher than the baseline and most of the SOTA methods. RobustSurg outperformed baseline by 3.74%, and 4.01% in terms of mIoU and mDSC scores. Similarly, our model surpassed other SOTA methods by a considerable margin. BlindNet performed slightly higher on mIoU and mDSC with 91.93% and 95.79% respectively. On the OOD setting, our method performed much better with mIoU score of 86.91% and 93.00% which is 43% and 38% higher than the baseline on both mIoU and mDSC scores both, and 2% and 1.1% better than BlindNet method on the same metrics.

Fig. 11 shows the qualitative performance of different methods on EndoUDA Barret's and polyp datasets. It can be observed that RobustSurg is able to achieve clearer segmentation boundaries and can work well on small as well as large polyps.

Results on CaDIS and Cataract-1K Benchmark: Table 10 presents the quantitative performance of SOTA and our method on Cataract surgery datasets. On the CaDIS test set, our proposed model outperforms the baseline by 1.6% on mIoU score and 2.8% on mDSC score, and achieves better results than most of the SOTA method, for instance 1.23% higher mIoU, 1.6% higher mDSC score on second best method. On the Cataract-1K OOD dataset, our proposed model outperforms the baseline by 51.2% and 35.3% in terms mIoU and mDSC scores. Our method achieves 3.9% higher mIoU and 8.2% higher mDSC as compared to the second best method (BlindNet).

Fig. 12 presents the qualitative performance on indomain and out-of-domain cataracts datasets. Most method

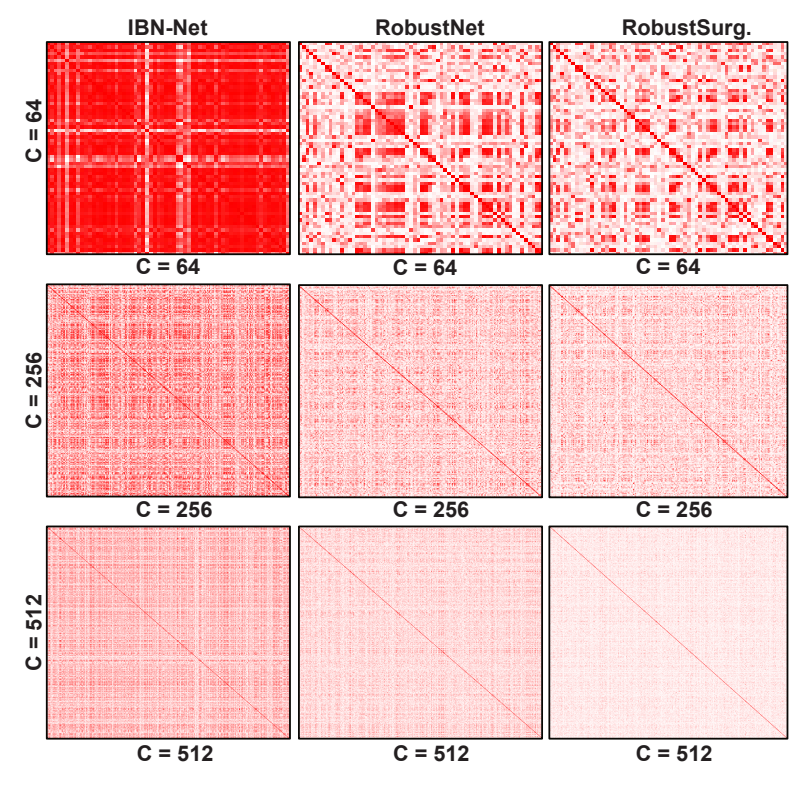


Figure 10: Visualization of covariance matrices extracted from IBN- Net, RobustNet and our model. The first, second and third rows represent feature covariance matrices extracted from the first, the second and third convolution layers, respectively.

Table 9
Table showing mean Intersection over Union (mIoU), Dice, Precision, Recall and accuracy scores for the SOTA and our proposed method on EndoUDA dataset. Best values are represented in **Bold** and second best underlined.

| EndoUDA (polyp)              |   | Test (IID)                              |       |       |   | Target (OOD)                            |       |       |
|------------------------------|---|---|-------|-------|---|---|-------|-------|
| Method                       | mloU                                    | mDSC                                    | Prec. | Rec.  | mloU                                    | mDSC                                    | Prec. | Rec.  |
| Baseline Chen et al. (2018)  | $81.42 \pm 0.551$                       | $90.32 \pm 0.234$                       | 90.21 | 90.11 | $64.28 \pm 0.350$                       | $73.45 \pm 0.234$                       | 77.88 | 76.84 |
| IBN-Net Pan et al. (2018)    | $\overline{77.08} \pm \overline{0.671}$ | $\overline{87.45} \pm \overline{0.534}$ | 89.01 | 85.59 | $68.04 \pm 0.230$                       | $76.21 \pm 0.452$                       | 86.34 | 75.63 |
| RobustNet Choi et al. (2021) | $78.18 \pm 0.310$                       | $89.33 \pm 0.457$                       | 90.46 | 85.51 | $70.24 \pm 0.871$                       | $78.34 \pm 0.332$                       | 91.18 | 75.65 |
| SNR Jin et al. (2021)        | $81.06 \pm 0.176$                       | $89.31 \pm 0.421$                       | 88.00 | 91.13 | $71.37 \pm 0.120$                       | $80.40 \pm 0.321$                       | 88.72 | 77.89 |
| SAN-SAW Peng et al. (2022)   | $74.59 \pm 0.325$                       | $85.45 \pm 0.347$                       | 86.12 | 84.79 | $46.04 \pm 0.412$                       | $63.05 \pm 0.383$                       | 67.57 | 59.10 |
| SAMed Zhang and Liu (2023)   | $79.32 \pm 0.231$                       | $88.45 \pm 0.356$                       | 88.42 | 83.76 | $74.12 \pm 0.154$                       | $82.78 \pm 0.347$                       | 89.30 | 72.55 |
| BlindNet Ahn et al. (2024)   | $78.20 \pm 0.110$                       | $87.77 \pm 0.630$                       | 86.72 | 88.84 | $\overline{53.49} \pm \overline{0.237}$ | $\overline{69.70} \pm \overline{0.161}$ | 78.94 | 62.40 |
| RobustSurg (Ours)            | $\textbf{81.67} \pm \textbf{0.871}$     | $\textbf{91.54} \pm \textbf{0.243}$     | 89.22 | 91.32 | $78.30 \pm 0.111$                       | $\textbf{89.69} \pm \textbf{0.321}$     | 89.96 | 86.93 |
| EndoUDA (BE)                 |   |   |       |       |   |   |       |       |
| Baseline Chen et al. (2018)  | $88.20 \pm 0.764$                       | $91.34 \pm 0.521$                       | 93.87 | 93.63 | $60.73 \pm 0.410$                       | $67.23 \pm 0.621$                       | 70.21 | 65.82 |
| IBN-Net Pan et al. (2018)    | $76.82 \pm 0.842$                       | $80.41 \pm 0.440$                       | 82.35 | 85.21 | $68.38 \pm 0.421$                       | $75.82 \pm 0.460$                       | 80.31 | 73.62 |
| RobustNet Choi et al. (2021) | $84.23 \pm 0.621$                       | $88.39 \pm 0.342$                       | 91.45 | 90.61 | $71.36 \pm 0.341$                       | $81.90 \pm 0.42$                        | 81.57 | 75.54 |
| SAMed Zhang and Liu (2023)   | $86.88 \pm 0.463$                       | $92.25 \pm 0.419$                       | 93.96 | 91.61 | $75.20 \pm 0.538$                       | $82.75 \pm 0.503$                       | 79.36 | 85.70 |
| SNR Jin et al. (2021)        | $85.37 \pm 0.333$                       | $89.49 \pm 0.478$                       | 92.54 | 91.73 | $72.87 \pm 0.551$                       | $83.43 \pm 0.320$                       | 84.24 | 76.72 |
| SAN-SAW Peng et al. (2022)   | $87.59 \pm 0.387$                       | $93.39 \pm 0.352$                       | 93.52 | 93.25 | $70.53 \pm 0.346$                       | $82.71 \pm 0.421$                       | 78.00 | 84.30 |
| BlindNet Ahn et al. (2024)   | $91.93 \pm 0.540$                       | $95.79 \pm 0.301$                       | 96.03 | 95.56 | $85.15 \pm 0.420$                       | $91.98 \pm 0.251$                       | 91.47 | 92.49 |
| RobustSurg (Ours)            | $91.50 \pm 0.530$                       | $95.01 \pm 0.409$                       | 97.06 | 93.35 | $86.91 \pm 0.461$                       | $\overline{93.00} \pm \overline{0.273}$ | 95.08 | 91.00 |

work well in segmenting anatomical landmarks on the CadIS dataset, but struggle to accurately segment instrument classes such as Irrigation-Aspiration. However, our method is able to provide more accurate segmentation boundaries for all the classes. Results on the Cataract-1K dataset are only shown for two classes, where our method can perform

better segmentation of Iris and Pupil, but other methods suffer from over-segmentation.

# 5.8. Discussion

Domain generalisation is being extensively investigated in the natural image domain through various methods including style-content disentanglement frameworks (Choi

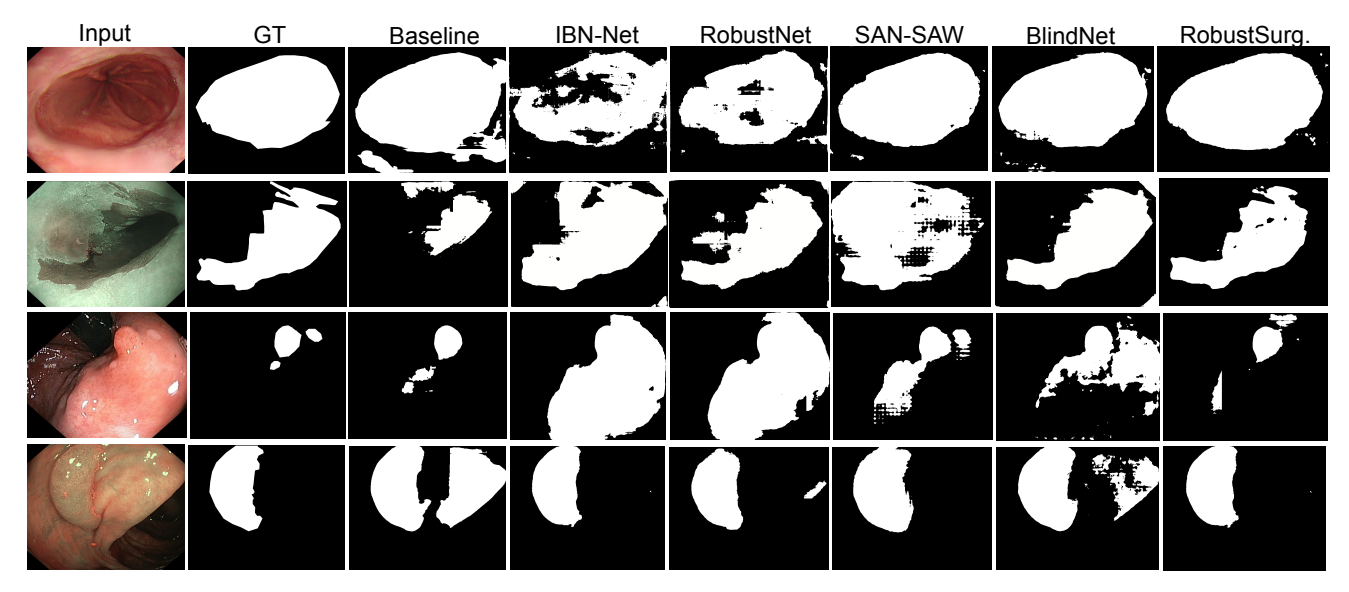


**Figure 11:** Qualitative results on EndoUDA BE and Polyp datasets. Top two rows contain qualitative performance on WLI and NBI BE images respectively while third and fourth rows contain WLI and NBI modality polyp images.

Table 10
Table showing mean Intersection over Union (mIoU), Dice, Precision, Recall and accuracy scores for the SOTA and our proposed method on cataract surgery datasets. Best values are represented in **Bold** and second best underlined.

|                              |  | CaDIS (IID)                            |       | Cataract-1K (OOD) |  |                  |              |       |
|------------------------------|--|--|-------|-------------------|--|------------------|--------------|-------|
| Method                       | mloU                                   | mDSC                                   | Prec. | Rec.              | mloU                                   | mDSC             | Prec.        | Rec.  |
| Baseline Chen et al. (2018)  | $73.64 \pm 0.76$                       | $82.46 \pm 0.72$                       | 83.13 | 85.48             | $29.92 \pm 0.75$                       | $43.09 \pm 0.65$ | 31.54        | 65.23 |
| IBN-Net Pan et al. (2018)    | $72.90 \pm 0.82$                       | $81.52 \pm 0.63$                       | 82.98 | 84.69             | $33.20 \pm 0.84$                       | $48.56 \pm 0.73$ | 35.60        | 69.89 |
| RobustNet Choi et al. (2021) | $73.06 \pm 0.84$                       | $83.33 \pm 0.63$                       | 83.26 | 84.40             | $41.58 \pm 0.72$                       | $52.63 \pm 0.70$ | 53.46        | 77.51 |
| SAMed Zhang and Liu (2023)   | $72.37 \pm 0.57$                       | $82.85 \pm 0.42$                       | 82.64 | 84.11             | $41.84 \pm 0.60$                       | $47.38 \pm 0.52$ | 43.68        | 56.60 |
| SNR Jin et al. (2021)        | $73.92 \pm 0.78$                       | $83.44 \pm 0.64$                       | 83.53 | 84.63             | $40.37 \pm 0.51$                       | $51.06 \pm 0.52$ | 49.37        | 73.53 |
| SAN-SAW Peng et al. (2022)   | $\overline{68.67} \pm \overline{0.60}$ | $\overline{79.83} \pm \overline{0.54}$ | 81.30 | 79.84             | $39.97 \pm 0.67$                       | $56.24 \pm 0.51$ | 62.34        | 54.30 |
| BlindNet Ahn et al. (2024)   | $71.56 \pm 0.95$                       | $81.92 \pm 0.76$                       | 83.43 | 82.49             | $43.54 \pm 0.63$                       | $53.87 \pm 0.54$ | 53.42        | 82.48 |
| RobustSurg (Ours)            | $\textbf{74.83} \pm \textbf{0.71}$     | $\textbf{84.78} \pm \textbf{0.50}$     | 84.81 | 85.39             | $\overline{45.26} \pm \overline{0.52}$ | $58.34 \pm 0.41$ | <u>55.16</u> | 77.68 |

et al., 2021; Zhao et al., 2022; Ahn et al., 2024), however, it is severely underexplored topic in the surgical domain. One important reason for this is the lack of availability of multicentre labeled datasets for the generalisability assessment of developed methods. To this end, we approach the domain generalisation problem from two perspectives, firstly, to address the important research gaps in the surgical domain having lack of diverse labeled datasets, we introduce a multicentre labeled dataset with pixel-wise annotations for the generalisability evaluation of methods, and secondly we introduce style-content disentanglement based on instance whitening transformation (Choi et al., 2021) from the natural domain to the surgical image domain by proposing RobustSurg method to effectively learn discriminative information to improve model generalisability.

As reported by prior works (Ahn et al., 2024; Jin et al., 2021) and pictorially depicted in Fig. 2, previous DG methods predominantly using instance normalisation to suppress the image styles also remove useful features from the training data. We aim to alleviate this problem by adding style normalisation and restitution module (Jin et al., 2021) before the feature whitening unlike performing the feature

whitening directly as reported in (Choi et al., 2021). Results on both in-domain and out-of-domain datasets as shown in Tables 2, 9, 10 validate the effectiveness of our approach. Results on the Cholecystectomy surgery dataset in Table 2 shows that our method substantially improved upon both RobustNet and SNR in both in-domain and out-domain cases showing the effectiveness of using feature restitution before performing feature whitening. For instance, on the in-domain dataset RobustSurg outperformed RobustNet by 1.8% and SNR by 1.2% in terms of mean IoU score. On the generalisability tests on HeiCholeSeg, RobustSurg demonstrates a mIoU score improvement of 6.44% and 5.54% on center 1, and 10.45%, 14.59% on center 2 compared to RobustNet and SNR methods respectively. This performance gain implies that combining feature restitution with instance whitening actually encourages the model in learning discriminant features for better domain generalisation and the restitution stage serves to effectively remove style information as depicted in Fig. 10. Methods such as SHADE, SNR and BlindNet do well on HeiCholeSeg centre 1, but their performance degrades on centre 2. This implies that they struggle to deal with a higher image resolution.

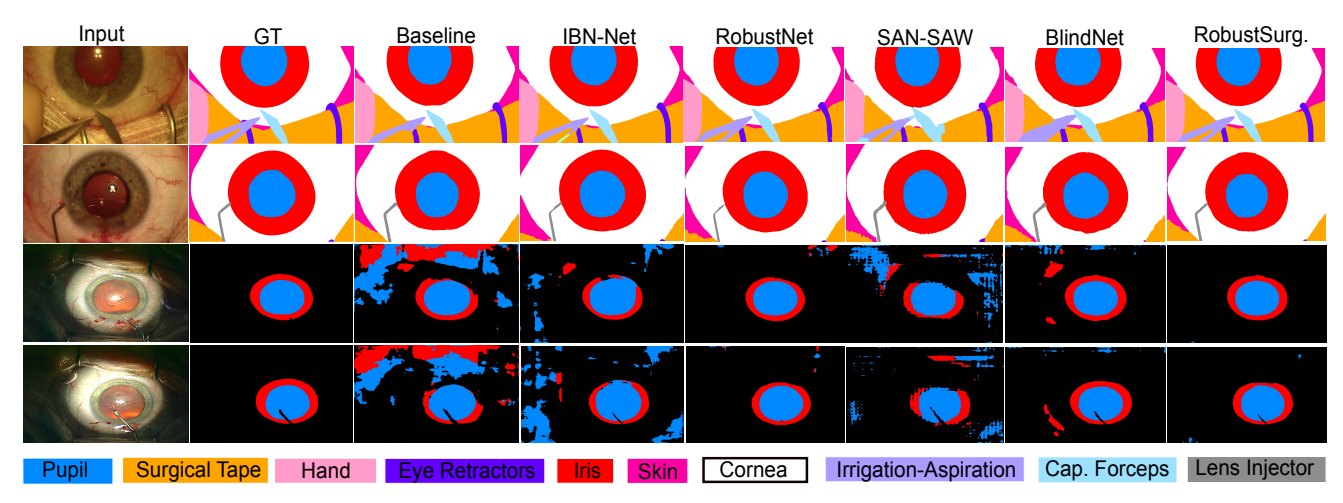


Figure 12: Qualitative results on CaDIS and cataract-1K datasets. Top two rows depict the qualitative performance on CaDIS and Cataract-1K data images respectively.

However, our method shows consistent performance in both centres demonstrating its robustness to the image resolutions. As RobustSurg essentially exploits the feature space in the feature extraction backbone, we also show in Table 5 that our method consistently outperforms other SOTA on other important backbone networks such as MobileNetv2 and ShuffleNetv2 making RobustSurg a backbone-agnostic method. In Fig. 8, paired *t*-test shows RobustSurg achieved highly significant difference against other methods with narrower deviation on both in-domain and out-of-domain datasets demonstrating robust performance of our method.

We observe the similar performance trends on other dataset setting, such as multi-modality EndoUDA dataset in Table 9 where training and test data come from a different modality. For example, RobustSurg surpassed RobustNet and SNR by 11.47% and 9.7% in terms of IoU score on EndoUDA polyp target set, and 21.79%, and 19.26% on EndoUDA Barrett's oesophagus target set in terms of IoU score. RobustSurg also demonstrates a consistent improvement in all evaluation metrics on cataract surgery datasets as shown in Table 10. For instance on CaDIS in-domain test set, RobustSurg obtained 2.4% and 1.2% higher IoU score compared to the RobustNet and SNR, and similarly on OOD Cataract-1K dataset, RobustSUrg outperformed RobustNet and SNR by 8.9% and 12% in terms of IoU score.

# 6. Conclusion and future directions

In this work, we addressed the DG problem for surgical scene segmentation by addressing the weaknesses in the IN and WT. We propose a domain-invariant feature encoder where we integrate a restitution network to restore the discriminant information lost due to the instance normalisation, and ISW block to selectively suppress the style information and retain content useful for the model generalisability. We used DeepLabv3+ as the base model for semantic segmentation with ResNet50 as the backbone. We comprehensively

evaluated our method on various datasets including laparoscopic and cataract surgery and an endoscopic data. We have also addressed the lack of multicentre data to evaluate model generalization by introducing a pixel-level annotated dataset named HeiCholeSeg, comprising of data from two different centres. Overall results on individual datasets shows the strong generalization performance of our method. To improve model performance on individual classes and address the performance degradadation on instrument classes due to vendor differences, we will work on individual class specific learning paradigms inside the segmentation decoder in future.

# Acknowledgments

The authors wish to acknowledge the Mexican Secretaría de Ciencia, Humanidades, Tecnología e Innovación (Secihti) for their support in terms of postgraduate scholarships in this project, and the Data Science Hub at Tecnologico de Monterrey for their support on this project.

This work has been supported by Azure Sponsorship credits granted by Microsoft's AI for Good Research Lab through the AI for Health program. The project was also supported by the French-Mexican ANUIES CONAHCYT Ecos Nord grant 322537, the WUN Research Development Fund 2024, the Crohn's & Colitis UK (M2023-5) and the Academy of Medical Sciences (SBF0010\1191). This work was also partially supported by the Worldwide Universities Network (WUN) Research Development Fund 2022 on "Novel robust computer vision methods and synthetic datasets for minimally invasive surgery" and Research Development Fund 2024 on "Artificial Intelligence for Surgical Training Towards Safer and Effective Sub-mucosal Dissection".

License agreement for HeiChole benchmark was published under Creative Commons Attribution-NonCommercial-ShareAlike (CC BY-NC-SA)

#### References

- Ahn, W.J., Yang, G.Y., Choi, H.D., Lim, M.T., 2024. Style blind domain generalized semantic segmentation via covariance alignment and semantic consistence contrastive learning, in: Proceedings of the ieee/cvf conference on computer vision and pattern recognition, pp. 3616–3626.
- Akbar, M.U., Wang, W., Eklund, A., 2025. Beware of diffusion models for synthesizing medical images—a comparison with gans in terms of memorizing brain mri and chest x-ray images. Machine Learning: Science and Technology 6, 015022.
- Bar, O., Neimark, D., Zohar, M., Hager, G.D., Girshick, R., Fried, G.M., Wolf, T., Asselmann, D., 2020. Impact of data on generalization of ai for surgical intelligence applications. Scientific reports 10, 22208.
- Blanchard, G., Lee, G., Scott, C., 2011. Generalizing from several related classification tasks to a new unlabeled sample. Advances in neural information processing systems 24.
- Buia, A., Stockhausen, F., Hanisch, E., 2015. Laparoscopic surgery: A qualified systematic review. World journal of methodology 5, 238.
- Carlucci, F.M., D'Innocente, A., Bucci, S., Caputo, B., Tommasi, T., 2019.
  Domain generalization by solving jigsaw puzzles, in: Proceedings of the IEEE/CVF conference on computer vision and pattern recognition, pp. 2229–2238.
- Celik, N., Ali, S., Gupta, S., Braden, B., Rittscher, J., 2021. Endouda: a modality independent segmentation approach for endoscopy imaging, in: International Conference on Medical Image Computing and Computer-Assisted Intervention, Springer. pp. 303–312.
- Cha, J., Chun, S., Lee, K., Cho, H.C., Park, S., Lee, Y., Park, S., 2021.Swad: Domain generalization by seeking flat minima. Advances in Neural Information Processing Systems 34, 22405–22418.
- Chen, L.C., Zhu, Y., Papandreou, G., Schroff, F., Adam, H., 2018. Encoder-decoder with atrous separable convolution for semantic image segmentation, in: Proceedings of the European conference on computer vision (ECCV), pp. 801–818.
- Cho, W., Choi, S., Park, D.K., Shin, I., Choo, J., 2019. Image-to-image translation via group-wise deep whitening-and-coloring transformation, in: Proceedings of the IEEE/CVF Conference on Computer Vision and Pattern Recognition, pp. 10639–10647.
- Choi, S., Jung, S., Yun, H., Kim, J.T., Kim, S., Choo, J., 2021. Robustnet: Improving domain generalization in urban-scene segmentation via instance selective whitening, in: Proceedings of the IEEE/CVF Conference on Computer Vision and Pattern Recognition, pp. 11580– 11590
- Gatys, L., Ecker, A.S., Bethge, M., 2015. Texture synthesis using convolutional neural networks. Advances in neural information processing systems 28.
- Gatys, L.A., Ecker, A.S., Bethge, M., 2016. Image style transfer using convolutional neural networks, in: Proceedings of the IEEE conference on computer vision and pattern recognition, pp. 2414–2423.
- Gong, R., Li, W., Chen, Y., Gool, L.V., 2019. Dlow: Domain flow for adaptation and generalization, in: Proceedings of the IEEE/CVF conference on computer vision and pattern recognition, pp. 2477–2486.
- Grammatikopoulou, M., Sanchez-Matilla, R., Bragman, F., Owen, D., Culshaw, L., Kerr, K., Stoyanov, D., Luengo, I., 2024. A spatiotemporal network for video semantic segmentation in surgical videos. International Journal of Computer Assisted Radiology and Surgery 19, 375-382
- Gresele, L., Von Kügelgen, J., Stimper, V., Schölkopf, B., Besserve, M., 2021. Independent mechanism analysis, a new concept? Advances in neural information processing systems 34, 28233–28248.
- Gu, R., Wang, G., Lu, J., Zhang, J., Lei, W., Chen, Y., Liao, W., Zhang, S., Li, K., Metaxas, D.N., et al., 2023. Cddsa: Contrastive domain disentanglement and style augmentation for generalizable medical image segmentation. Medical Image Analysis 89, 102904.
- Guo, S., Luo, H., Zhu, Y., Zhao, F., 2023. Style semantic disentangle network for multi-source domain generalization, in: 2023 IEEE 8th International Conference on Big Data Analytics (ICBDA), IEEE. pp. 31–38
- Guo, X., Liu, J., Yuan, Y., 2024. Infproto-powered adaptive classifier and agnostic feature learning for single domain generalization in medical

- images. International Journal of Computer Vision, 1-24.
- Hong, W.Y., Kao, C.L., Kuo, Y.H., Wang, J.R., Chang, W.L., Shih, C.S., 2020. Cholecseg8k: a semantic segmentation dataset for laparoscopic cholecystectomy based on cholec80. arXiv preprint arXiv:2012.12453.
- Igaki, T., Kitaguchi, D., Matsuzaki, H., Nakajima, K., Kojima, S., Hasegawa, H., Takeshita, N., Kinugasa, Y., Ito, M., 2023. Automatic surgical skill assessment system based on concordance of standardized surgical field development using artificial intelligence. JAMA surgery, e231131–e231131.
- Jin, X., Lan, C., Zeng, W., Chen, Z., 2021. Style normalization and restitution for domain generalization and adaptation. IEEE Transactions on Multimedia 24, 3636–3651.
- Labelbox, 2024. Labelbox: Training Data Platform for Machine Learning. https://labelbox.com/. Accessed: 2025-05-07.
- Lee, S., Seong, H., Lee, S., Kim, E., 2022. Wildnet: Learning domain generalized semantic segmentation from the wild, in: Proceedings of the IEEE/CVF Conference on Computer Vision and Pattern Recognition, pp. 9936–9946.
- Li, Y., Fang, C., Yang, J., Wang, Z., Lu, X., Yang, M.H., 2017. Universal style transfer via feature transforms. Advances in neural information processing systems 30.
- Mascagni, P., Alapatt, D., Garcia, A., Okamoto, N., Vardazaryan, A., Costamagna, G., Dallemagne, B., Padoy, N., 2021. Surgical data science for safe cholecystectomy: a protocol for segmentation of hepatocystic anatomy and assessment of the critical view of safety. arXiv preprint arXiv:2106.10916.
- Mascagni, P., Vardazaryan, A., Alapatt, D., Urade, T., Emre, T., Fiorillo, C., Pessaux, P., Mutter, D., Marescaux, J., Costamagna, G., et al., 2022. Artificial intelligence for surgical safety: automatic assessment of the critical view of safety in laparoscopic cholecystectomy using deep learning. Annals of surgery 275, 955–961.
- Mathieu, M.F., Zhao, J.J., Zhao, J., Ramesh, A., Sprechmann, P., LeCun, Y., 2016. Disentangling factors of variation in deep representation using adversarial training. Advances in neural information processing systems 29.
- Murali, A., Alapatt, D., Mascagni, P., Vardazaryan, A., Garcia, A., Okamoto, N., Costamagna, G., Mutter, D., Marescaux, J., Dallemagne, B., et al., 2023. The endoscapes dataset for surgical scene segmentation, object detection, and critical view of safety assessment: Official splits and benchmark. arXiv preprint arXiv:2312.12429.
- Nam, H., Kim, H.E., 2018. Batch-instance normalization for adaptively style-invariant neural networks. Advances in Neural Information Processing Systems 31.
- Nguyen, A.T., Tran, T., Gal, Y., Baydin, A.G., 2021. Domain invariant representation learning with domain density transformations. Advances in Neural Information Processing Systems 34, 5264–5275.
- Pan, X., Luo, P., Shi, J., Tang, X., 2018. Two at once: Enhancing learning and generalization capacities via ibn-net, in: Proceedings of the European Conference on Computer Vision (ECCV), pp. 464–479.
- Pan, X., Zhan, X., Shi, J., Tang, X., Luo, P., 2019. Switchable whitening for deep representation learning, in: Proceedings of the IEEE/CVF International Conference on Computer Vision, pp. 1863–1871.
- Peng, D., Lei, Y., Hayat, M., Guo, Y., Li, W., 2022. Semantic-aware domain generalized segmentation, in: Proceedings of the IEEE/CVF conference on computer vision and pattern recognition, pp. 2594–2605.
- Peters, J., Janzing, D., Schölkopf, B., 2017. Elements of causal inference: foundations and learning algorithms. The MIT Press.
- Philipp, M., Alperovich, A., Gutt-Will, M., Mathis, A., Saur, S., Raabe, A., Mathis-Ullrich, F., 2021. Localizing neurosurgical instruments across domains and in the wild, in: Medical Imaging with Deep Learning.
- Philipp, M., Alperovich, A., Gutt-Will, M., Mathis, A., Saur, S., Raabe, A., Mathis-Ullrich, F., 2022. Dynamic cnns using uncertainty to overcome domain generalization for surgical instrument localization, in: Proceedings of the IEEE/CVF Winter Conference on Applications of Computer Vision, pp. 3612–3621.
- Ross, T., Reinke, A., Full, P.M., Wagner, M., Kenngott, H., Apitz, M., Hempe, H., Filimon, D.M., Scholz, P., Tran, T.N., et al., 2020. Robust medical instrument segmentation challenge 2019. arXiv preprint

- arXiv:2003.10299.
- Roy, S., Siarohin, A., Sangineto, E., Bulo, S.R., Sebe, N., Ricci, E., 2019. Unsupervised domain adaptation using feature-whitening and consensus loss, in: Proceedings of the IEEE/CVF conference on computer vision and pattern recognition, pp. 9471–9480.
- Satyanaik, S., Murali, A., Alapatt, D., Wang, X., Mascagni, P., Padoy, N., 2024. Optimizing latent graph representations of surgical scenes for unseen domain generalization. International Journal of Computer Assisted Radiology and Surgery, 1–8.
- Seenivasan, L., Islam, M., Ng, C.F., Lim, C.M., Ren, H., 2022. Biomimetic incremental domain generalization with a graph network for surgical scene understanding. Biomimetics 7, 68.
- Sharma, S., Nwoye, C.I., Mutter, D., Padoy, N., 2023. Rendezvous in time: an attention-based temporal fusion approach for surgical triplet recognition. International Journal of Computer Assisted Radiology and Surgery, 1–7.
- Sun, X., Wu, B., Zheng, X., Liu, C., Chen, W., Qin, T., Liu, T.Y., 2021. Recovering latent causal factor for generalization to distributional shifts. Advances in Neural Information Processing Systems 34, 16846–16859.
- Szabó, A., Hu, Q., Portenier, T., Zwicker, M., Favaro, P., 2017. Challenges in disentangling independent factors of variation. arXiv preprint arXiv:1711.02245.
- Ulyanov, D., Vedaldi, A., Lempitsky, V., 2016. Instance normalization: The missing ingredient for fast stylization. arXiv preprint arXiv:1607.08022
- Venkatesh, D.K., Rivoir, D., Pfeiffer, M., Kolbinger, F., Speidel, S., 2025.Data augmentation for surgical scene segmentation with anatomy-aware diffusion models, in: 2025 IEEE/CVF Winter Conference on Applications of Computer Vision (WACV), IEEE. pp. 2280–2290.
- Wagner, M., Müller-Stich, B.P., Kisilenko, A., Tran, D., Heger, P., Mündermann, L., Lubotsky, D.M., Müller, B., Davitashvili, T., Capek, M., et al., 2023. Comparative validation of machine learning algorithms for surgical workflow and skill analysis with the heichole benchmark. Medical Image Analysis 86, 102770.
- Wang, A., Islam, M., Xu, M., Zhang, Y., Ren, H., 2023. Sam meets robotic surgery: An empirical study on generalization, robustness and adaptation, in: International Conference on Medical Image Computing and Computer-Assisted Intervention, Springer. pp. 234–244.
- Wei, G., Lan, C., Zeng, W., Chen, Z., 2021. Metaalign: Coordinating domain alignment and classification for unsupervised domain adaptation, in: Proceedings of the IEEE/CVF conference on computer vision and pattern recognition, pp. 16643–16653.
- Xu, L., Zhang, H., Wang, J., Li, A., Song, S., Ren, H., Qi, L., Gu, J.J., Meng, M.Q.H., 2023. Information loss challenges in surgical navigation systems: From information fusion to ai-based approaches. Information Fusion 92, 13–36.
- Yoon, J., Hong, S., Hong, S., Lee, J., Shin, S., Park, B., Sung, N., Yu, H., Kim, S., Park, S., et al., 2022. Surgical scene segmentation using semantic image synthesis with a virtual surgery environment, in: International Conference on Medical Image Computing and Computer-Assisted Intervention, Springer. pp. 551–561.
- Zhang, B., Goel, B., Sarhan, M.H., Goel, V.K., Abukhalil, R., Kalesan, B., Stottler, N., Petculescu, S., 2023. Surgical workflow recognition with temporal convolution and transformer for action segmentation. International Journal of Computer Assisted Radiology and Surgery 18, 785–794.
- Zhang, K., Liu, D., 2023. Customized segment anything model for medical image segmentation. arXiv preprint arXiv:2304.13785.
- Zhao, Y., Zhong, Z., Zhao, N., Sebe, N., Lee, G.H., 2022. Style-hallucinated dual consistency learning for domain generalized semantic segmentation, in: European conference on computer vision, Springer. pp. 535–552.
- Zhou, K., Yang, Y., Hospedales, T., Xiang, T., 2020. Learning to generate novel domains for domain generalization, in: Computer Vision–ECCV 2020: 16th European Conference, Glasgow, UK, August 23–28, 2020, Proceedings, Part XVI 16, Springer. pp. 561–578.
- Zhou, K., Yang, Y., Qiao, Y., Xiang, T., 2021. Domain generalization with mixstyle. arXiv preprint arXiv:2104.02008.